NASA/TP—2017-219413

SBIR Advanced Technologies in Aviation and Air Transportation System 2016

Hung D. Nguyen and Gynelle C. Steele
Glenn Research Center, Cleveland, Ohio

January 2017

NASA STI Program . . . in Profile

Since its founding, NASA has been dedicated to the advancement of aeronautics and space science. The NASA Scientific and Technical Information (STI) Program plays a key part in helping NASA maintain this important role.

The NASA STI Program operates under the auspices of the Agency Chief Information Officer. It collects, organizes, provides for archiving, and disseminates NASA's STI. The NASA STI Program provides access to the NASA Technical Report Server—Registered (NTRS Reg) and NASA Technical Report Server—Public (NTRS) thus providing one of the largest collections of aeronautical and space science STI in the world. Results are published in both non-NASA channels and by NASA in the NASA STI Report Series, which includes the following report types:

- TECHNICAL PUBLICATION. Reports of completed research or a major significant phase of research that present the results of NASA programs and include extensive data or theoretical analysis. Includes compilations of significant scientific and technical data and information deemed to be of continuing reference value. NASA counter-part of peer-reviewed formal professional papers, but has less stringent limitations on manuscript length and extent of graphic presentations.

- TECHNICAL MEMORANDUM. Scientific and technical findings that are preliminary or of specialized interest, e.g., "quick-release" reports, working papers, and bibliographies that contain minimal annotation. Does not contain extensive analysis.

- CONTRACTOR REPORT. Scientific and technical findings by NASA-sponsored contractors and grantees.

- CONFERENCE PUBLICATION. Collected papers from scientific and technical conferences, symposia, seminars, or other meetings sponsored or co-sponsored by NASA.

- SPECIAL PUBLICATION. Scientific, technical, or historical information from NASA programs, projects, and missions, often concerned with subjects having substantial public interest.

- TECHNICAL TRANSLATION. English-language translations of foreign scientific and technical material pertinent to NASA's mission.

For more information about the NASA STI program, see the following:

- Access the NASA STI program home page at http://www.sti.nasa.gov

- E-mail your question to help@sti.nasa.gov

- Fax your question to the NASA STI Information Desk at 757-864-6500

- Telephone the NASA STI Information Desk at 757-864-9658

- Write to:
  NASA STI Program
  Mail Stop 148
  NASA Langley Research Center
  Hampton, VA 23681-2199

NASA/TP—2017-219413

SBIR Advanced Technologies in Aviation and Air Transportation System 2016

Hung D. Nguyen and Gynelle C. Steele
Glenn Research Center, Cleveland, Ohio

National Aeronautics and
Space Administration

Glenn Research Center
Cleveland, Ohio 44135

January 2017

Level of Review: This material has been technically reviewed by expert reviewer(s).

Available from

NASA STI Program
Mail Stop 148
NASA Langley Research Center
Hampton, VA 23681-2199

National Technical Information Service
5285 Port Royal Road
Springfield, VA 22161
703-605-6000

This report is available in electronic form at http://www.sti.nasa.gov/ and http://ntrs.nasa.gov/

Preface

The Small Business Innovation Research (SBIR) program was established under the Small Business Innovation Development Act of 1982 (P.L. 97-219) to strengthen the role of innovative small business concerns in Federally funded research and development (R&D) projects. This highly competitive program encourages domestic small businesses to engage in Federal research and development projects that have the potential for commercialization.

NASA SBIR and Small Business Technology Transfer (STTR) programs fund research, development, and demonstration of innovative technologies that fulfill NASA needs as described in the annual solicitations and have significant potential for successful commercialization.

This report is a compilation of various topics associated with NASA's Aeronautics Research Mission Directorate (ARMD), with particular emphasis on the NASA SBIR contracts awarded to small companies from 2011 to 2012. The technologies highlighted in this report focus on high-quality, cutting-edge research that will lead to revolutionary concepts, technologies, and capabilities that will fundamentally change both the airspace system and the aircraft that fly within it, thus facilitating a safer, more environmentally friendly, and more efficient air transportation system.

It is anticipated that this report will provide opportunities for NASA engineers, researchers, and program managers to learn how NASA SBIR technologies could help their programs and projects, and lead to more collaborations and partnerships between small SBIR companies and NASA that would benefit both. This report also targets and will serve as a valuable reference for researchers, academia, students, other scientists, and government.

Contents

Chapter 1—An Enhanced Plasma Actuator for Compressor Stall Control

Richard W. Kaszeta and Calman Gold
Creare LLC
Hanover, New Hampshire 03755

Thomas C. Corke, Ryan McGowan, and Eric Matlis
University of Notre Dame
Notre Dame, Indiana 46556

1.1 Introduction

Interest in dielectric barrier discharge (DBD) plasma actuators for flow control has seen a tremendous growth in the past 15 years in the U.S. and around the world. The likely reasons for this are based on special features such as being fully electronic with no moving parts, having a fast time response for unsteady applications, having a very low mass which is especially important in applications with high g-loads, being able to apply the actuators onto surfaces without the addition of cavities or holes, and having efficient conversion of the input power without parasitic losses when properly optimized.

Traditionally, DBD actuators consist of two electrodes, one coated and one uncoated and exposed to the air and encapsulated by a dielectric material, and are excited with an AC voltage at high (kV) levels that causes weak ionization of the gas over the air. Inducing motion of the charged ions and electrons of the plasma field then can induce a body force on the flow over the electrode. This body force, while generally efficient at producing thrust with no moving parts, has been limited by two factors: (1) limited thrust produced by the actuators themselves, and (2) difficulty in implementation actuation circuits that can efficiently convert supply voltage into the desired actuation waveform.

Creare LLC and the University of Notre Dame (UND) have developed a new technique for DBD actuation that uses a DC-based actuation circuit that is capable of producing both substantially increased thrust while reducing implementation and integration issues in the resulting system.

1.2 Identification and Significance of the Innovation

To achieve stall-free operation in conventional engine systems, current compressor designs require that stall pressure ratio capability exceed the steady state and transient requirements by 10 to 30%. This stall margin ultimately requires extra stages of compression that increase weight and cost while adversely impacting aerodynamic performance. Active compressor stall control has the potential to reduce the required number of stages of compression, thereby reducing the weight, part count, and cost. Reducing the stall margin will allow operation at the highest efficiency while reducing CO_2, NO_x, and particulate emissions. The optimized DBD plasma actuation circuit enables substantially increased thrust which in turn enables the use of DBD actuators for active flow control in applications such as compressor stall control where the limited thrust of traditional DBD actuators has limited the use of this technique. Creare and UND are developing a demonstration system for compressor flow control that is expected to substantially improve stall control in modern compressor engines.

1.3 Technical Concept and Development

Creare and UND have developed a micropulsed DC plasma actuator designed to produce substantially enhanced thrust over traditional DBD actuators while substantially improving system size, weight, and power. This hybrid approach combines the best aspects of existing AC and DC plasma actuators. Figure 1.1 shows a capacitor charging circuit that is driven from rectified 120 Vac current and a high-voltage metal-oxide semiconductor field-effect transistor MOSFET switch array that supplies both the high DC voltage and periodic switching necessary for DBD actuator operation. As Figure 1.2 shows, the DC source is fed to both electrodes. A resistor, R, limits the current to the lower electrode, which is also connected to a fast-acting solid-state switch that when closed, shorts the voltage to the lower electrode to the earth ground, producing a sharp leading edge of a reverse-voltage pulse followed by a gradual RC decay of the circuit back to the unexcited state. The resulting voltage and current waveforms across the actuator are shown in Figure 1.2. These waveforms correspond to a supply voltage, V_{ddH} = 7 kV and an actuation frequency of 1,000 Hz for a 2.5-in. long actuator. There are similar time series for every thrust measurement data point that will appear in subsequent figures. Figure 1.2 shows two simultaneous voltage time traces. The trace with the sharp downward peaks, is labeled V_{drain5}, is measured at the drain of the last power MOSFET in the chain output of the solid-state switch and corresponds to the voltage time series that is fed to the covered electrode of the plasma actuator. The other voltage time trace, labeled V_{ddH}, corresponds to the DC voltage that is supplied to the exposed electrode of the plasma actuator. Figure 1.2 corresponds to the time series of the current being fed to the covered electrode of the plasma actuator. This waveform is intended to maximize thrust by several mechanisms: (1) the sharp leading edge of the circuit allows rapid formation of a strong plasma field, (2) the slower trailing edge of the RC decay allows the plasma field to be maintained without collapsing an creating an anti-thrust, and (3) a modest DC offset component between the electrodes similarly enhances thrust production by maintaining a constant stream of positive ions.

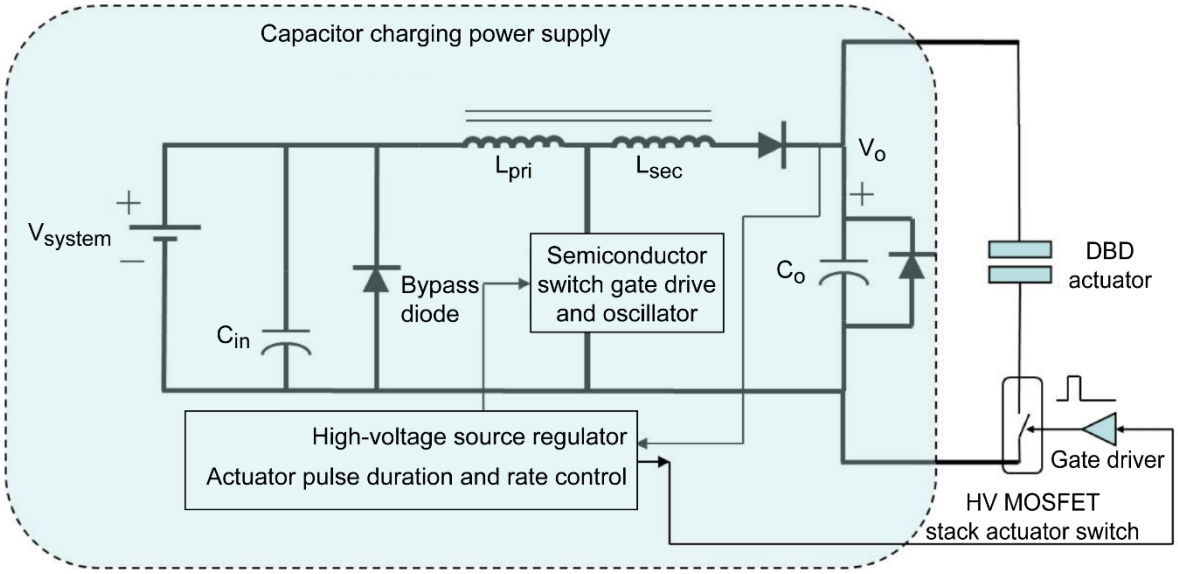

Figure 1.1.—Micropulsed DC actuator system showing power conversion and high-voltage switching components.

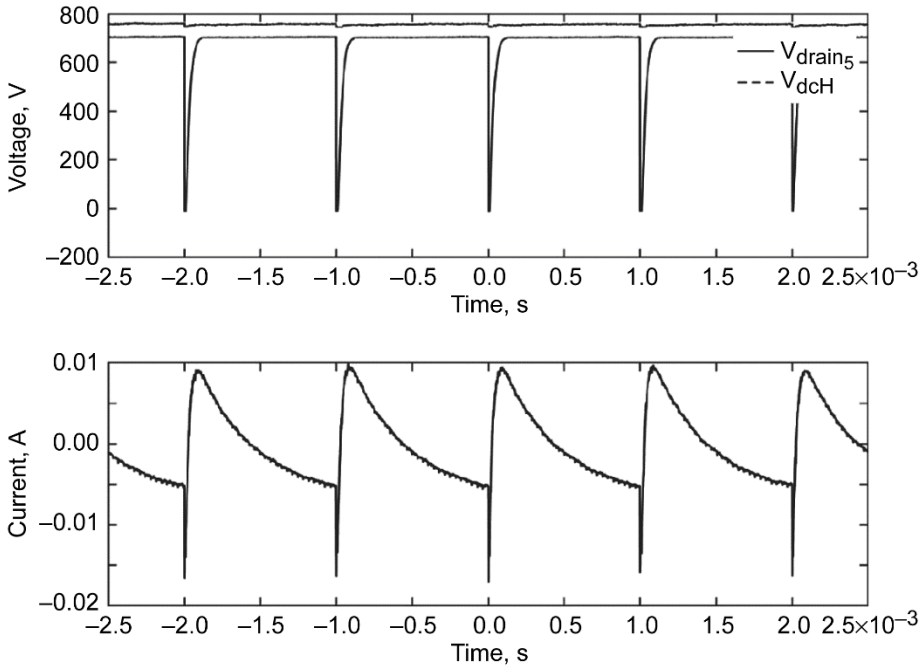

Figure 1.2.—Representative waveforms of a 7-kV supplied voltage, 1,000 Hz actuation frequency and a 2.5-in. Kapton actuator.

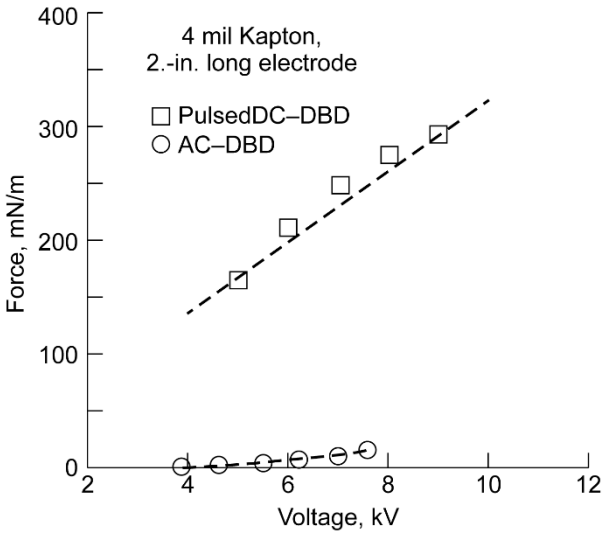

Figure 1.3.—Comparison of the induced thrust measured from both AC–DBD and micropulsed DC with 4 mil Kapton, 2.5-in. actuators.

Experiments were performed to document the induced thrust produced by a DBD plasma actuator mounted on a force measuring scale. The plasma actuator consisted of electrodes that were 2.5 in. long and the dielectric layer consisted of two, 2-mil thick layers of Kapton (DuPont) film. The actuator was operated with a traditional AC input or with a pulsed-DC input as shown in Figure 1.2. The two approaches were categorized in terms of the amount of induced thrust produced by the two plasma actuator arrangements. The results are shown in Figure 1.3. The voltage scale is peak-to-peak voltage for AC operation and DC voltage for the pulsed-DC operation. The monitored temperature and humidity in the lab were 71 °F and 35% relative humidity.

The AC plasma actuator thrust displays the characteristic power law relation $T \sim V^{3.5}$. In contrast, the pulsed DC generated thrust is linear with the input DC voltage. Most notably, the thrust generated by the pulsed-DC operation is more than an order of magnitude larger than that produced by AC operation. In fact, the pulsed-DC thrust levels shown in Figure 1.3 are greater than any thrust levels documented with AC plasma actuators that occurred at ten times higher voltages. Although a Kapton dielectric was used in previous sample thrust measurements, Kapton is generally not suitable for experiments that operate for long periods of time, since it is degraded by the O_3 generated by the plasma. Another dielectric material we have used is Ultem (Plastics International) film, which is a polyetherimide (PEI) that is not affected by exposure to O_3. It has a dielectric strength of approximately 3 kV/mil, which we verified in tests. The dielectric strength of Ultem film is approximately half that of the Kapton film. Traditionally, Ultem has not been used much for high-thrust DBD applications due to this reduced dielectric strength, but because this is not a critical issue with the lower voltages used in pulsed-DC operation, we performed experiments to compare the thrust generated with the Ultem film dielectric against those with the

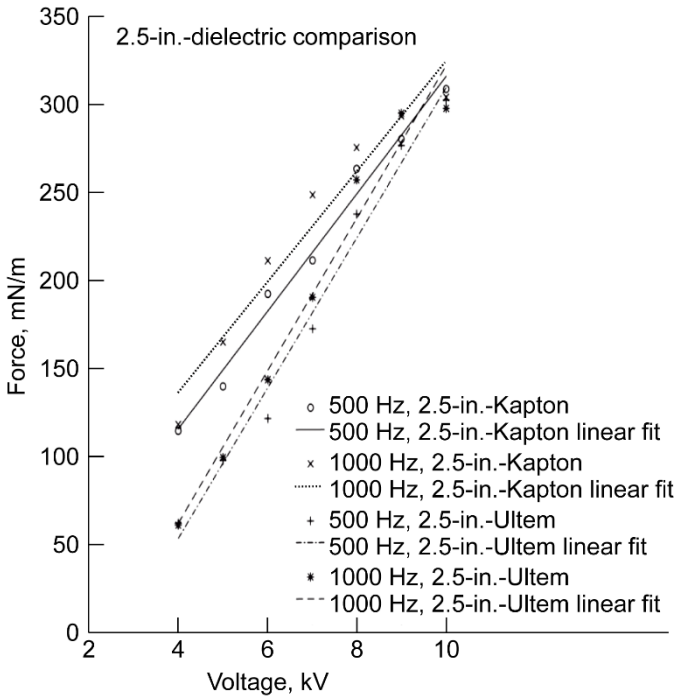

Figure 1.4.—Dielectric comparison of 2.5-in. Ultem and Kapton actuators.

Kapton film. The thickness of the Ultem film used in these experiments was 3 mil. The thrust comparison between the Ultem and Kapton dielectric materials with the 2.5-in.-long actuators is shown in Figure 1.4. Two pulsed-DC frequencies of 500 and 1000 Hz are presented. In general, the thrust produced with the Ultem dielectric was less than that with the Kapton at the lower voltages. The change in the thrust with voltage was higher with the Ultem so that at the higher voltages, the thrust produced with the two different dielectric materials were comparable.

Using an Ultem-based DBD actuator design, Creare and UND are now fabricating a compressor test facility that applies axial thrust to the compressor shroud casing in the tip clearance gap. We expect these actuators to provide a substantially improved stall margin. Those results will be published once completed.

1.4 Target Markets

There is clear demand for improved stall control systems in commercial turbine engine compressor systems. To achieve stall-free operation in conventional engine systems current compressor designs require that stall pressure ratio capability exceed the steady state and transient requirements by 10 to 30%. This stall margin ultimately requires extra stages of compression that increase the weight and cost while adversely impacting aerodynamic performance. Active compressor stall control has the potential to reduce the required number of compression stages, thereby reducing weight, part count, and cost. Reducing the stall margin will allow operation at the

highest efficiency, as well as reducing CO_2, NO_x, and particulate emissions. The techniques presented here are also expected to be applicable to the Wind Turbine community. The unsteady nature of wind power makes transient stall a major performance issue in modern wind turbines. Like compressor stall, the primary approach to eliminating stall in wind turbines involves designing systems with substantial stall margin. However, an active flow control system, such as that developed here, has the potential to allow active stall suppression on wind turbine blades, and allow the turbine to be operated much closer to optimal conditions with substantial reduced stall margin.

1.5 Applications

The advantages of the micropulsed DBD actuator system compared to competing technology imply that it has potential markets in both compressor stall control and general aerodynamics. Customers include all current and emerging turbine engine manufacturers for propulsion and power generation applications, existing rotorcraft manufacturers, and wind turbine developers. The time to market in most cases will be paced by concurrent technology development in alternative flow control strategies, primarily research efforts based on passive flow control techniques. The nearest term applications are likely to be in compressor stall control, although active research is currently taking place in these other areas of interest.

1.6 Conclusion

A novel actuation circuit for improving the thrust generated by DBD actuators has been demonstrated. The results indicate that for the same input voltage and frequency, a six times greater thrust occurred with this technique versus traditional AC operation. The advantage of the pulsed-DC plasma actuator is the ability to achieve very high body force levels at considerably lower voltages. This makes it much easier to incorporate into active flow control applications. The new pulsed-DC plasma actuator has been implemented for stall control in a test facility at NDU, and a substantial increase in stall margin is expected.

Chapter 2—Next Generation High-Resolution Autostereoscopic Display

Jesse Eichenlaub
Dimension Technologies Inc.
Rochester, New York 14611

2.1 Introduction

2.1.1 How a Next Generation Autostereoscopic Glasses-Free 3D Liquid Crystal Display (LCD) Will Make Air Travel Safer

In the Next Generation Air Transportation System, pilots will receive better information from their autostereoscopic instrumentation and navigation displays (Ref. 2.1). According to NASA, this will result in an 18% improvement in pilot situational awareness.

Air traffic controllers will have a better intuitive understanding and greater command of their airspace because they will see air traffic on their displays with high-fidelity depth cues. Luggage screeners will have far greater knowledge of what is in each bag and will be more effective and efficient in their jobs because they will be able to see the image on their screens in real-depth stereo.

People who make mission-critical decisions and take actions based in large part on what they see on their liquid crystal displays (LCDs) will be able to see two-dimensional (2D) images like they always do, and will be able to see three-dimensional (3D) images like never before—in full resolution, full brightness, without glasses or headsets.

How will they be able to do this? With a next-generation autostereoscopic glasses-free 3D LCD commissioned by NASA through the SBIR program and designed and built by Dimension Technologies Inc. (DTI) of Rochester, New York.

2.2 Identification and Significance of the Innovation

The science has been in for a long time—depth matters!

NASA studies dating back to the 1990s have proven conclusively that pilots perform better in critical aviation procedures when they are presented with navigation information and instrumentation in realistic 3D.

> "I have been a researcher and consultant for government and industry in the field of stereoscopic 3D image capture and display for over 30 years. Many scientific studies and a wealth of real-world experience have shown that 3D displays can improve human performance in mission-critical situations. For example, 3D displays can improve a pilot's awareness of conditions and other aircraft in surrounding airspace, and can provide enhanced warning capabilities when a hazardous situation is encountered."
>
> —John O. Merritt, Senior Consulting Scientist, The Merritt Group (merritt.com)

So what does an 18% improvement in situational awareness mean? Let's consider a high-stakes scenario—a mid-air-collision avoidance maneuver. U.S. Naval Aviation Safety Center research shows that it takes 12.5 sec from the time the anomaly is first identified to the time that the plane responds to the pilot's action (Figure 2.1).

Two commercial airliners traveling at 500 mph have an effective closing speed of 1000 mph—that is a mile every 3.6 sec. If you spot the anomaly 4 miles out, you have to beat the average by 2.0 sec.

In this scenario, an 18% improvement in situational awareness could very well make the difference between a successful avoidance and a tragic collision.

3D provides critical slope and terrain information for low-level flying, landing, and taxiing. 3D enables improved performance for critical life-saving maneuvers such as "hover in turbulence for helicopters" (Ref. 2.2), and improved remote operation for unmanned aviation systems.

It is fair to say that in this scenario and many others, the DTI glasses-free 3D display has the potential to save lives. The one thing that is certain, the pilot in this scenario would want to be making that decision in real time with the best available information. In the next generation, that means LCDs that have DTI glasses-free 3D technology inside.

2.3 Technical Concept and Development

DTI's High-Resolution Autostereoscopic Cockpit Display has six key features that are all required and unique (as a group) to meet NASA's demanding performance goals:

- Glasses-free 3D viewing
- Ability to display as much depth as 3D glasses without the glasses
- Ability to display both 2D and 3D images at the full resolution of the display
- Ability to switch dynamically between 2D and 3D image display modes
- Freedom of head movement when viewing 3D
- A power-efficient LED back-lit display with a wide range of brightness from extremely dim to sunlight readable

DTI's system sends light through the LCD so that the two eyes see all of the LCD pixels at different times. When the light goes through the pixels to the left eye, the pixels display the left eye view of a stereo pair; when light goes through the pixels to the right eye, the pixels display the right eye view of a stereo pair. This happens fast enough so that no flicker is seen, thus

Figure 2.1.—Improved situational awareness can make the difference in a high-stakes scenario.

the user sees a true stereoscopic image. Internal firmware in the display makes sure that the lights and image display on the LCD pixels stay in sync with each other. The lighting system and related optics in the backlight are designed to send light to two observers simultaneously. An onboard eye tracking system will keep track of where the observers are and make sure that the light is aimed at their eyes.

The display will use the same type of field sequential output that is used when viewing with 3D shutter glasses—a left eye view followed by a right eye view every 1/120th of a second.

2.4 Target Markets and Key Applications

NASA's interest in this project is primarily for improving commercial transport aircraft safety. However, based on extensive research and numerous field demonstrations, the DTI glasses-free 3D display will be of potential benefit in a number of high-value and/or high-volume applications for NASA, government, and commercial enterprises. Applications include the following:

Aerospace
- Cockpit and flight deck displays
- Air traffic control and airspace monitoring
- Unmanned systems (drones) remote navigation and operation

Automotive
- Driver instrument clusters
- Center console displays

Education
- Classrooms and study labs
- Training and simulation

Government
- Military command and control
- Training and simulation
- Telerobotic systems
- Luggage screening

Research
- Biomolecular
- Chemical
- Data visualization and analysis
- Pharmaceutical
- Geophysical mapping

DTI's strategy is to license its intellectual property IP (trademarked DTI ROC 3D) to major monitor manufacturers who will mass produce 3D displays with DTI ROC3D technology inside, making them available to NASA and others at low cost for a variety of applications.

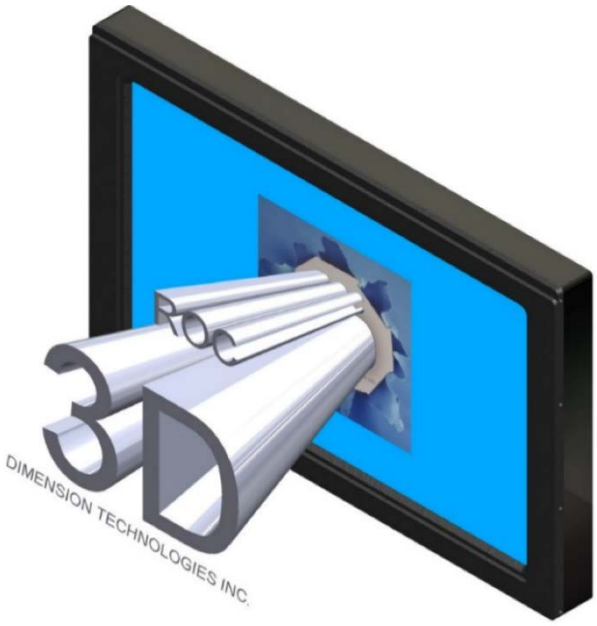

Figure 2.2.—A breakthrough in autostereoscopic technology.

DTI is currently developing commercial solutions for an aerospace and an automotive customer (both are world leaders and innovators in their respective markets), and will have a near-product prototype of a 15.6-in. LCD display available by January 2017 (Figure 2.2).

2.5 Conclusion

Researchers at the U.S. Air Force Research Laboratory, in Dayton, Ohio examined 162 studies involving 184 experiments comparing human performance using 2D displays and 3D displays for vital tasks including spatial understanding of complex scenes; spatial manipulation of objects; and finding, identifying, and classifying objects. The findings were conclusive—3D improves human performance (Ref. 2.3)!

NASA and DTI have long known about the potential of glasses-free 3D. We developed our first display in the early 90s. It was crude and expensive, but it worked. We advanced the technology over the next 20 years, earning induction into the NASA Space Technology Hall of Fame and a Hallmark of Success designation.

Now the technology has advanced, the costs have come down dramatically and the market is ready for the next generation in glasses-free 3D—DTI ROC 3D is going to deliver it.

2.6 References

2.1. Williams, Steven P.; Parrish, Russell V.; and Busquets, Anthony M: Benefits, Limitations, and Guidelines for Application of Stereo 3–D Display Technology to the Cockpit Environment. Presented at the NATO, AGARD Conference on Advanced Aircraft Interfaces: The Machine Side of the Man Machine Interface, Madrid, Spain, 1992.

2.2. Stereopsis Cueing Effects on Hover-in-Turbulence Performance in a Simulated Rotorcraft. NASA TP–2980, 1990. http://ntrs.nasa.gov

2.3. McIntire, John P.; Havig, Paul R.; and Geiselman, Eric E.: Stereoscopic 3–D Displays and Human Performance: A Comprehensive Review. Displays, vol. 35, no. 1, 2014, pp. 18–26.

Chapter 3—Deployable Engine Air-Brake for Drag Management Applications

Joshua T. Davis and Parthiv N. Shah
ATA Engineering, Inc.
San Diego, California 92128

3.1 Introduction

ATA Engineering, Inc. has developed and demonstrated a novel aircraft drag management technology known as an engine air-brake (EAB) that promises to support the goals of NASA and the aircraft industry for next-generation quiet aircraft. Aircraft noise issues in the communities surrounding airports have long been a concern, however, developing noise mitigation methods for aircraft without decreasing performance or fuel economy has proven challenging. ATA's EAB has been designed to address these challenges through the use of a deployable swirl vane mechanism to switch the operation of a turbofan engine nozzle from conventional mode to a "drag management" mode. In this mode, swirling outflow from the thrust-generating exhaust stream allows an aircraft to generate equivalent drag in the form of engine thrust reduction at a fixed fan rotor speed. Thus the EAB has the potential to reduce community noise exposure by enabling aircraft to perform descents and approaches slower, aerodynamically cleaner, or steeper and thereby distancing the sound source from the community. But because the EAB stows to be aerodynamically neutral, it does not affect normal operation during cruise. Moreover, the technology also has the potential to result in a net fuel burn reduction by reducing the duration of the descent and approach phases of flight.

A 27-month Phase II SBIR project sponsored by the Acoustics Branch at NASA Glenn Research Center culminated in successful ground testing of the device on a Williams International FJ44-4 turbofan engine (Figure 3.1). However, the development of the patented EAB technology has been the product of over a decade of research. From an initial concept of a static, ram-air-driven "swirl tube" at MIT, ATA matured the EAB through a campaign of nozzle testing to its current state. The full-scale prototype resulted from an analysis-driven design effort that included optimization studies such as steady and unsteady computational fluid dynamics to quantify flow performance and operability, thermal and conjugate heat transfer analysis to predict thermal operating environments, structural dynamics to ensure strength and durability, and computer-aided mechanical design of the deployment mechanism. The prototype EAB was designed to fit within a notional engine cowl of an aircraft using the Williams International's FJ44-4 mixed-flow turbofan engine. Future technology maturation efforts will consist of further ground testing necessary to demonstrate durability and reliability, and eventual flight testing.

3.2 Identification and Significance of the Innovation

Takeoff and approach are the two events responsible for the most aircraft community noise exposure. Takeoff is dominated by noise from the engine at high power, while on approach airframe noise competes with and often exceeds engine noise due to the aerodynamic exposure of structures such as landing gear, high-lift devices, control surfaces, and speedbrakes. These structures all generate drag, which may generate significant noise. This motivates the need for "quiet" drag devices that may be deployed on approach to reduce noise through flight paths that are slower, aerodynamically cleaner, or steeper (thereby distancing the sound source from the community).

In particular, aviation authorities have sought development of steeper and/or slower descent and approach trajectories for noise reduction. Typical transport aircraft glideslopes are around 3° unless modified by local requirements, but steeper descent maneuvers and their potentially beneficial impact on noise have shown promise. Steeper maneuvers require additional drag to maintain the aircraft's approach speed to avoid adversely impacting noise and landing distance. The thrust generated by the engines at their approach power settings opposes the drag that is sought to achieve these operational benefits. Simply reducing the engine power during approach to reduce thrust (which is a form of equivalent drag) is generally not possible, however, because of the requirement of a minimum spool-up time to ensure safe go-around during aborted landings. Similarly, during descent, engines often produce excess thrust due to requirements such as high-temperature bleed air for aircraft anti-icing systems.

To provide a solution for reducing thrust while maintaining normal approach and descent engine speed, ATA developed a technology known as an engine air-brake (EAB). As shown in Figure 3.2, the EAB is a deployable (and rapidly stowable) device that positions vanes in the bypass flow or in the exhaust flow (in the case of a mixed-flow engine) of a turbofan engine. The EAB generates a swirling outflow from the engine's nozzle, allowing the aircraft to generate equivalent drag in the form of thrust reduction at a fixed fan rotor speed. The drag generated by the swirling exhaust flow is sustained by the strong radial pressure gradient created by the swirl vanes (Figure 3.3).

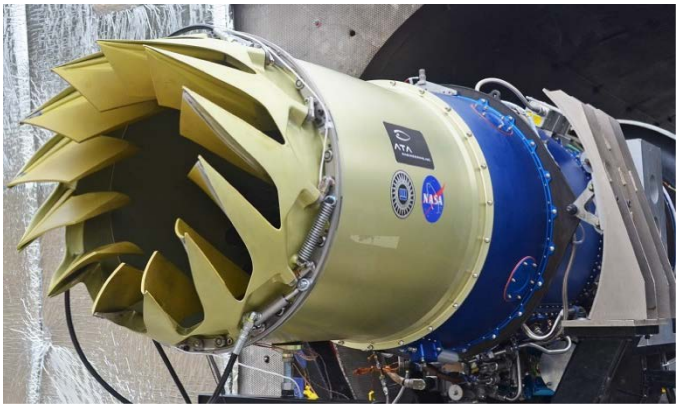

Figure 3.1.—Engine air-brake during full-scale demonstration testing on Williams International FJ44–4 turbofan engine.

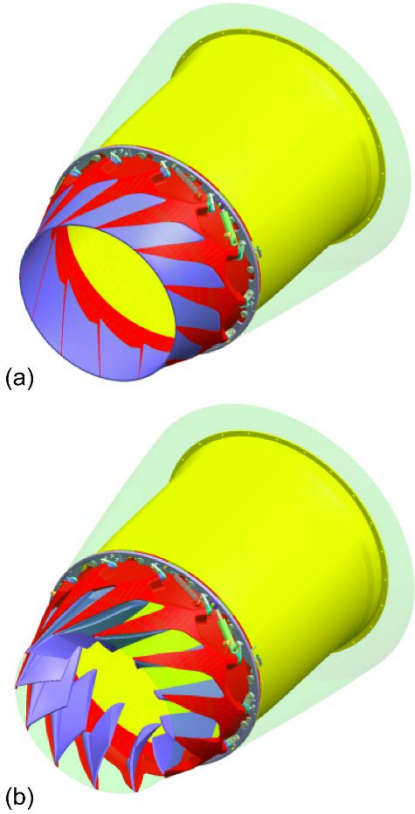

Figure 3.2.—EAB in (a) stowed and (b) deployed conditions.

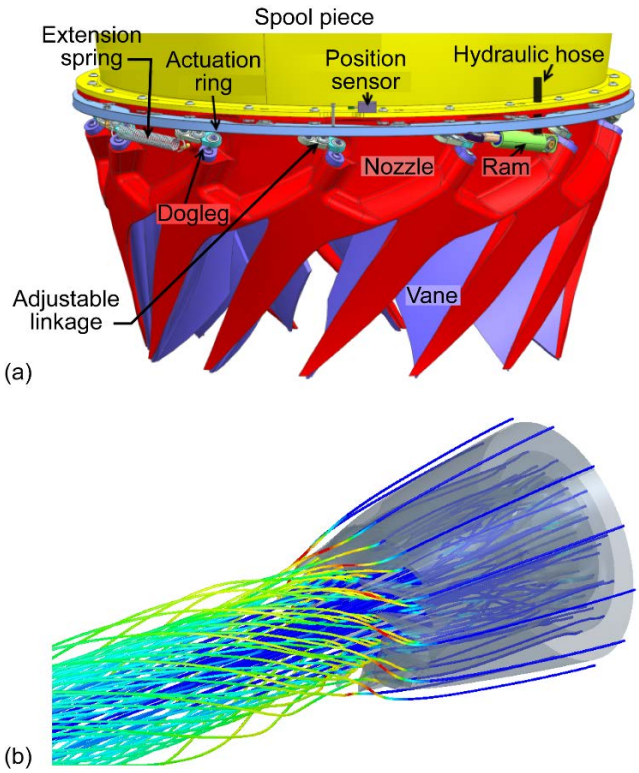

Figure 3.3.—Rendering of (a) EAB actuation hardware and (b) CFD simulation showing effect of swirl vanes on exhaust flow.

3.3 Technical Concept and Development

Technical development and demonstration of the technology occurred during two NASA-funded SBIR initiatives: a concept development program (CDP) from 2008 to 2011 and a system demonstration program (SDP) from 2012 to 2015. The CDP began with development of design concepts and progressed to the design, implementation, and operation of several aerodynamic prototypes in NASA Glenn's Aero-Acoustic Propulsion Laboratory (AAPL). In quantifying the relationship between swirl, flow, drag, and noise, aircraft-on-approach noise simulations were used to demonstrate that an appropriately designed EAB could enable a steep approach trajectory (from a baseline 3.2° glideslope to 4.4°) for a 737-800-class aircraft at a fixed speed. A peak tone-corrected perceived noise level (PNLT) reduction of up to 3.1 dB was predicted at the ground observer location, with a potential 1.8 dB effective perceived noise level (EPNL[1]) reduction. The CDP culminated in a prototype paper design for a swirl vane deployment mechanism that would remain stowed and aerodynamically "invisible" to the bypass flow path during conventional operation and would then deploy a set of vanes projecting inward from the fan nozzle casing surface during drag management maneuvers.

[1]While EPNL is not a steep approach certification metric, it is used here as a figure of merit for comparison.

The SDP involved design, fabrication, and testing of a realistic flight-weight EAB prototype on a modern turbofan propulsion system. ATA collaborated with Williams International, a leading manufacturer of powerplants for the light business jet market, leading to the selection of the FJ44–4A mixed-flow turbofan (used aboard the Cessna CJ4 and the Pilatus PC-24) as the engine platform for the demonstration. Design of the EAB prototype was driven by extensive structural and aerodynamic analysis to ensure that the device safely met intended performance specifications. Structural analysis involved static, dynamic, and finite element analysis of the components subject to the vibration and heat of the engine exhaust environment. ATA performed several rounds of computational fluid dynamics (CFD) simulation to optimize the EAB's ability to create equivalent drag without impacting engine operation when deployed, and ensure that it would not cause any reduction in thrust when stowed.

The SDP effort culminated in testing of the EAB prototype on a full-scale engine test cell at Williams International's Outdoor Test Facility #2, shown in Figure 3.4. The primary engine testing objectives were to

1. Measure the performance of the stowed and deployed EAB to quantify the equivalent drag via thrust reduction,
2. Determine the effective flow capacity (to assess the impact of the EAB on engine operation),
3. Assess the change in near- and far-field noise, and
4. Demonstrate controlled deployment and stowing within specified durations.

Secondary objectives included monitoring stresses on the swirl vanes and other components to assess structural design margins and confirm part life.

3.4 Key Outcomes

The final prototype design (Figure 3.4) satisfied a set of critical technology demonstration requirements that included

1. Aerodynamic equivalent drag production equal to 15% of thrust in a high-powered approach throttle setting (called dirty approach)
2. Excess nozzle flow capacity and fuel burn reduction in the fully deployed configuration
3. Acceptable engine operability during dynamic deployment and stowing
4. Deployment time of 3 to 5 sec
5. Stowing time under 0.5 sec
6. Packaging of the mechanism within a notional engine cowl

For a typical twin-jet aircraft application, a constant-speed, steep approach analysis suggests that the EAB drag could be used without additional external airframe drag to increase the conventional glideslope from 3° to 4.3°, with about 3 dB noise reduction at a fixed observer location.

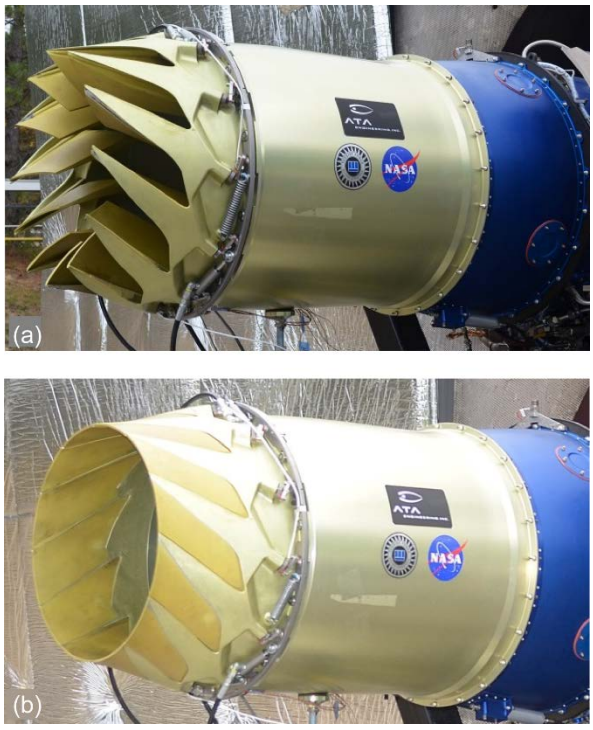

Figure 3.4.—EAB prototype during on-engine testing in (a) deployed and (b) stowed configurations.

3.5 Target Markets

Target markets for the EAB include commercial passenger, military transport, and business jet aviation applications. Stakeholders involved in its adoption may include airport authorities, airline operators, airframers, and aircraft owners.

Aircraft noise is regulated globally by the International Civil Aviation Organization, but it is often increasing local requirements that dictate key elements of the design of aircraft for lower noise, and influential airport authorities will continue to push for enabling technologies for noise reduction. Significant successes on continuous-descent approaches (CDAs) have brought these procedures into more frequent use. For instance, London Heathrow (LHR) Airport's 2015 "Blueprint for Noise Reduction" includes both a campaign for quiet approaches focused on CDAs and exploration of steeper angles of descent as two of its top ten practical steps to cut noise. The EAB may be a critical enabler for these envisioned flight protocols.

In addition, the EAB may enable greater access to geographically confined airports. For instance, authorities have certified a steep approach for the Airbus A318 at London City (LCY) Airport, providing the operator (British Airways) with a competitive advantage of landing transatlantic flights at a regional airport. Similarly, reducing landing distance (i.e., short-field performance) would enable access to more airports, a capability particularly appealing to business jet owners who demand convenience. As the EAB prototype was designed and validated for a business jet engine platform, aircraft developed

by Cessna, HondaJet, Gulfstream, Bombardier, and others may present the most realizable initial target market. Potential customers include both the aforementioned aircraft companies and their engine suppliers (e.g., Honeywell, Pratt and Whitney, Williams International, and GE Aviation).

3.6 Applications

Two potential commercial applications exist for the EAB technology: (1) implementation as a complementary technology in retrofit on older aircraft engines to meet current and future noise requirements and (2) implementation in future jet engines as an integral part of the engine design, i.e., incorporation of exhaust nozzles with a variable mechanism that generates a swirling outflow in drag management mode. Retrofit application provides a simpler and faster implementation and is an opportunity to demonstrate the effectiveness of the technology to the community before adoption by engine original equipment manufacturers.

3.7 Conclusions and Outlook

ATA Engineering in collaboration with NASA Glenn Research Center and Williams International, has demonstrated the potential of an engine air-brake technology to reduce noise exposure to communities near airports and enable greater access to confined airports. Testing of a full-scale EAB on a production turbofan engine showed that it could create sufficient thrust reduction to enable steeper approach profiles, which would locate noise sources farther from observers on the ground, and does not negatively impact normal engine operation. These benefits are expected to be applicable to business jets, large commercial aircraft, and military transports.

Having achieved a technology readiness level (TRL) of 6 through ground test demonstration of the prototype, future efforts will involve flight testing to further mature the technology and prepare it for commercialization. This activity will involve further optimization of the EAB design and integration into an experimental aircraft.

Chapter 4—Magnesium Diboride Superconductor Wire for Turboelectric Propulsion Systems

Matt Rindfleisch and Mike Tomsic
Hyper Tech Research
Columbus, Ohio 43228

Mike Sumption
The Ohio State University
Columbus, Ohio 43210

4.1 Introduction

Hyper Tech Research was awarded a Small Business Innovation Research (SBIR) Phase I and II contract based on a grant proposal submitted in response to NASA's call to seek "cutting-edge research in aeronautics to overcome technology barriers and challenges in developing highly efficient aircraft systems of the future, with limited impact to the environment." The solicitation stated that "turboelectric propulsion for aircraft applications is envisioned, and cryogenic and superconducting components are sought; and in particular, low AC loss superconducting materials for the stator windings are of interest."

There is an intense push in the aircraft industry to ultimately develop all-electric aircraft, with liquid hydrogen and fuel cells being considered as the prime generation source for aircraft propulsion. Today the U.S. finds itself in competition with Europe for the development of next generation all-electric aircraft. Superconductivity, especially magnesium diboride (MgB_2) superconductors, are considered an enabling technology that is being investigated by NASA, the U. S. Air Force, Rolls-Royce, Airbus, and European Aeronautic Defence and Space Company (EADS). Superconducting stators for motors and generators designed for these new platforms will need low cost, low AC loss superconductors that can operate in the 10 to 25 K temperature range in 0 to 2 Tesla fields. Wire is needed by 2016 to 2017 for fabricating cryogenic motors and generators that will be tested by NASA in 2017. Pursuant to these objectives, Hyper Tech introduced several innovations in wire manufacturing that advanced state-of-the-art low AC loss MgB_2-based conductors for turboelectric aircraft propulsion systems for future aircraft platforms.

4.2 Identification and Significance of the Innovation

Industry experts believe that the recent sharp increase in the cost of fuel occurring simultaneously with a relentless growth in air traffic will foster the development of revolutionary new aircraft technologies over the next 25 years (Ref. 4.1). New technologies include zero-emission aircraft, which will have to be developed in response to heightened environmental concerns. There is an intense push in the industry to ultimately develop an all-electric aircraft, with liquid hydrogen and fuel cells being considered as the prime generation source for aircraft propulsion. Consequently, the need to develop ultra-compact and light electric motors and actuators suitable for airborne applications is becoming increasingly urgent and critical.

NASA and the Department of Defense partnered with Georgia Tech to establish a University Research, Engineering, and Technology Institute on Aeropropulsion and Power Technology to develop a wide range of innovative propulsion and power technologies that will enable systems that meet highly restrictive local environmental (emissions and noise) regulations, burn less fuel to reduce global warming, improve safety beyond current levels, and exhibit lower acquisition and operating costs. An example of a design concept of next generation aircraft using turboelectric aircraft propulsion is NASA's N3-X configuration shown in Figure 4.1. The turboelectric approach requires that a number of new components (such as electric generators, transmission lines, motors, and possibly cryocoolers and inverters) be inserted into the aircraft propulsive drive train between the turbine engines and the propulsive fans. Most of these components must operate at very low temperatures to achieve flight weight at acceptable efficiency, adding to the number of technologies that must be evaluated. These include greater complexity and possible reliability issues, as well as the weight and inefficiencies introduced by added components. The penalties come in the form of additional fuel burn, which subtracts from the expected benefits, so the electrical system must not be too heavy or too inefficient. The generators, motors and transmission lines are all expected to be superconducting to achieve high power density and high efficiency. The aggregated component efficiencies are expected to be high, even with proper accounting of the power for the refrigeration system. The most obvious concern is the weight of the new components. A number of parametric studies were made on motors and generators that are optimized (with their coolers) for lowest weight. The results show the dependence of weight and efficiency on cryocooler weight per input power, on superconducting filament size, on superconducting wire size, and on the percentage of full load. It was shown that the sum of the weights of the motor, motor cooler, inverter, and inverter cooler falls below that of the baseline system for MgB_2 wire of small enough diameter, mainly due to the decrease in inverter weight from the baseline value (Ref. 4.2).

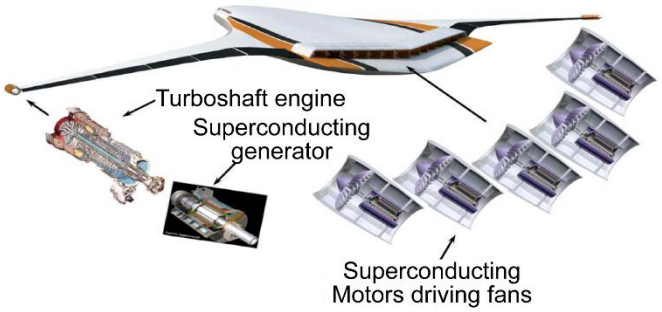

Figure 4.1.—Major turboelectric propulsion components for one concept of a blended-wing-body (BWB) aircraft, the N3-X.1 Wingtip mounted turboshaft engines drive superconducting generators that send power to an array of superconducting motors that drive propulsive fans. The motors and fans are embedded in a continuous nacelle.

A critical and enabling component of an all-cryogenic superconducting propulsion system is low AC loss superconductors that can operate in the 10 to 30 K range needed for the stator coils in the motors and generators. The amount of AC losses in the stator will determine the needed cooling capacity of the resulting superconducting stator coils. Compared with other families of superconductors, the intermediate-T_c (critical temperature) superconductor MgB_2 has several distinct advantages for use in AC applications including aircraft motors and generators:

1. Low cost
2. Low weight
3. Suitable engineering current density (J_e) in the desired operating temperature of 20 to 30 K (achievable by cryocooler or LH_2) (Ref. 4.3)
4. Available as round wire rather than flat tape, and therefore has the ability to be sized (amperage and J_e) to the desired power rating of the machine
5. Available in sufficient piece-length (order of km-long) and quantity (thousands of km per year) as shown in Figure 4.2
6. Most importantly can be configured to take advantage of commonly known conductor design techniques to lower AC losses, such as fine filaments (order of 10 μm), resistive filamentary matrix, small twist pitches, and multistrand braids and cables

Hyper Tech has been demonstrating MgB_2 superconductor wire products and manufacturing capacity for DC applications (magnetic resonance imaging (MRI), fault current limiters (FCL), and rotors in wind turbine generators), but conductor development for AC applications has been historically infrequent. Therefore the innovation of the SBIR project was to develop low AC loss MgB_2 superconductors and demonstrate the associated wire manufacturing capacity for turboelectric aircraft propulsion systems specifically for stator coils in the demonstration of a large (1 MW) fully superconducting electric machine.

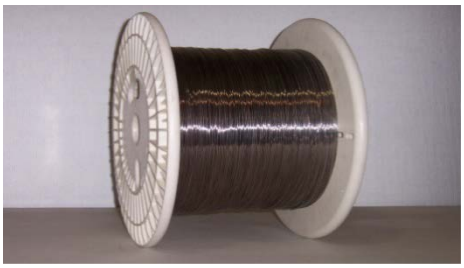

Figure 4.2.—Long length MgB_2 wire (specifically, 6 km length) wound on a storage spool.

4.3 Technical Concept and Development

Technical objectives concentrated on developing AC-tolerant MgB_2 superconductors designed for motor/generator stators for NASA's program to develop advanced turboelectric propulsion systems. Specific wire designs were based on parameters within NASA Glenn regimes of interest for a 1 MW fully superconducting electric machine demonstrator (with a 3-phase, 4-pole stator cooled with liquid hydrogen). AC loss in any kind of superconductor may arise from several sources—self-field loss in a conductor carrying an AC transport current, external-field-generated hysteresis loss in superconducting filaments, eddy current loss, and possible ferromagnetic loss in the sheath material and in the matrix. The SBIR project focused significant effort on configuring entirely new classes of MgB_2 superconductors with reduced hysteretic, coupling, and transport current loss components while concurrently meeting NASA specifications. New conductor designs were also analyzed for the ability to manufacture the AC tolerant superconductors in significant lengths and quality for coils. The project generated spools of low-AC loss MgB_2 wire for NASA and collaborators for designing future superconductor stator coils and wire samples for prototype stator coil development. Another end product of the SBIR project was that AC losses of MgB_2 superconductors were estimated based on measurements and modeling method custom-developed which would be useful for assisting engineers and scientists who plan to design stator coils and other cryogenic machines using MgB_2 wire. This technical paper describes the loss components in greater detail and how MgB_2 conductor development was driven to lower each AC loss component.

Hysteretic losses. The hysteresis losses are influenced by the geometry of the superconductor and direction and depth of the applied magnetic field; and they are directly proportional to current density and superconducting filament diameter. Significant effort was made in the SBIR project to develop multifilament MgB_2 wire of fine filament size of 10 μm or less (a goal stated by NASA) by increasing the number of filaments in the restack. The filament count and restack design determined the smallest effective filament diameter, d_{eff}, i.e., the smallest filament size that can be manufactured without a significant degradation of superconductivity properties. An

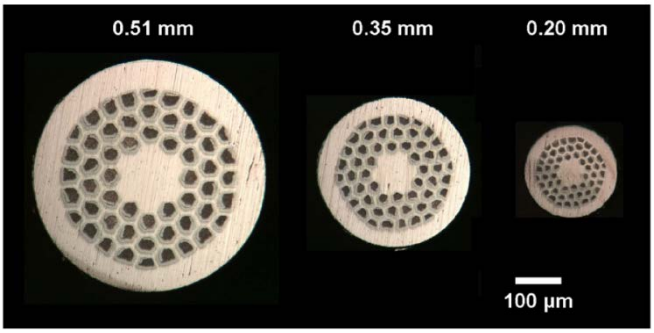

Figure 4.3.—A 54-filament MgB_2 conductor fabricated to progressively smaller wire diameters.

example of manufacturing a high filament count MgB_2 wire to progressively smaller wire diameters for producing fine filaments is illustrated in Figure 4.3. MgB_2 superconductors with very fine filaments in the 10 to 30 µm range were achieved by developing new wire designs of single-restack MgB_2 superconductors with filament counts as high as 192 and double restacks with 342 filaments as shown in Figures 4.4(a) and (b). High filament count single-restacks were typically made with a Cu10Ni filamentary matrix and either a Cu30Ni or 260 brass alloy outer sheath. Key to the success in fabricating these conductors with a large number of filaments was improving wire drawing techniques and the use of nanopowders in the filament. The greatest number of superconducting filaments in a single-restack that was successfully processed (wire drawn) to a d_{eff} of 10 µm without wire breaks, and characterized was 114. The double restack design is a multifilament strand whose filaments are another multifilament conductor instead of a monoelement or monofilament conductor as in the case of a single restack. The advantage of the double restack design is that 10 µm filaments can be obtained at a higher wire diameter, but disadvantages realized in the project were that the superconductor fraction was low and therefore corresponding I_c (critical current) would be lower, and a robust outer sheath was required to process (draw) the wire. Both single and double restacks fabricated with very fine filaments were demonstrated with good transport superconducting properties. Slight degradation in current density was realized when approaching a d_{eff} of 10 µm, however an increase in hysteretic losses with 20 µm filaments (which did not show degradation in J_c (critical current density)) would be relatively minor compared to other AC loss components, particularly coupling eddy current losses.

Coupling eddy current losses. In an AC-applied field, there is a loss generated by coupling currents that: (1) in the case of a multifilamentary strand, flow along the filaments and across the matrix (of resistivity ρ_{eff}), and (2) in the case of a cable, flow along the strands and across the points of contact between them. Coupling loss components include the frequency, external field, the twist pitch (L_p) and matrix resistivity of the conductor. MgB_2 conductor development for decreasing coupling losses

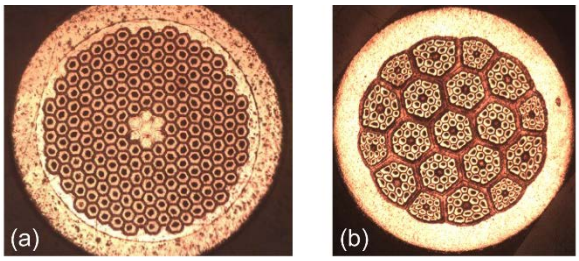

Figure 4.4.—(a) 192-filament MgB_2 and (b) 342-filament MgB_2. Conductors produced in this project.

included optimizing strand construction for reducing single-strand twist pitches as small as 5 mm in strands sized as large as 1 mm and modifying the wire architecture with higher resistive components (NASA's original wire specification was a 10-mm pitch). Twist pitch optimization studies were implemented whenever a new conductor developed in the project was successfully processed to the objective wire diameter and was found to have good superconductivity properties. The study focused on one strand sized to several wire diameters with corresponding superconducting filaments ranging from 10 to 30 µm that were twisted at various pitches between 5 and 100 mm. Twist pitch studies included 54-filament and 114-filament single restacks and a 342-filament double restack. Twist pitch optimization was also applied to larger 1-mm diameter wires as it became apparent that conductors needed to be sized larger to meet NASA specifications. MgB_2 superconductors for the first time were successfully single strand-twisted at a 5-mm twist pitch in this project, including the larger 1-mm wire. Another milestone achieved in the project is that no degradation in current density properties were observed in MgB_2 conductors with small 5- and 10-mm twist pitches although performance was influenced by wire diameter (some degradation was observed in samples sized larger than 0.7 mm). In general, all strands from the multiple twist pitch studies exhibited good superconductivity properties. Hyper Tech validated in this project two custom twisting machines designed and manufactured for processing MgB_2 superconductors. For example one machine used also for larger-diameter kilometer-length MRI wire, twisted a 0.96–mm 54-filament low AC loss wire at a 15 mm twist pitch with a length over 100 m. Another machine specifically designed for twisting and cabling fine wire (diameter < 0.5 mm) successfully twisted over 400 m of a 54-filament conductor sized to 0.31-mm with a 5-mm twist pitch.

Wire development also focused on the composition of the filamentary matrix since coupling losses are described to be inversely proportional to matrix resistivity. Since Hyper Tech's commercial MgB_2 wire products are made with a highly conductive copper filamentary matrix, the selection of replacement materials with higher resistivity for low AC loss conductor development had to meet three criteria: (1) the required mechanical properties for enabling wire drawing;

TABLE 4.1.—ESTIMATED AC LOSSES (IN TERMS OF W/cm^3) OF MgB_2 CONDUCTOR DESIGNED FOR NASA STATOR COILS

OD / d_{eff} / L_p (mm/μm/mm)	ρ_{eff}, μΩcm	J_C (0.45 T, 25 K), A/mm^2	I_{op}/I_C	I_C, A	f, Hz	Hyst (W/cm^3)	Coup (W/cm^3)	Trans (W/cm^3)	Total (W/cm^3)
0.85/28/5	11	2300	0.50	200	333	1.7	2.55	0.26	4.51

(2) available in practical size and form (e.g., tubing); and (3) available in reasonable quantities. The Nb chemical barrier is also part of the filamentary matrix, however as Nb remains the best chemical barrier between the Mg+B powders and remaining matrix material, this aspect of the conductor design was not changed. The strand architecture was successfully modified in new MgB_2 conductors by incorporating nickel-based copper alloys as the filamentary matrix material. Low AC loss MgB_2 conductors with high filament counts were successfully made with either a Cu10Ni or Cu30Ni filamentary matrix. These conductors were successfully processed to small d_{eff} and twist pitches and in long lengths. Resistivities of pure Cu, Cu10Ni and Cu30Ni are estimated at 20 K to be 0.02, 17, and 37 μΩcm, respectively. Selecting Cu30Ni over Cu10Ni would reduce coupling losses by over a factor of 2.

Estimated coupling losses also considered the operating frequency of the demonstrator. AC loss models showed that an increase of frequency from 200 to 333 Hz increased coupling loss by a factor of 2.8 (losses go as frequency squared).

Transport current losses. In prior work (Ref. 4.4), measured transfer current losses were found to be higher than losses estimated by modelling due to the field rerouting associated with the Monel (Special Metals Corporation; ~70%Ni, 30% Cu alloy) outer sheath, a material found to be slightly ferromagnetic. Materials sought to replace magnetic copper-nickel alloys needed to not only be nonmagnetic but also have high resistivity to reduce coupling losses, and if used as a matrix material, normal metal eddy current losses. Therefore, regarding the outer sheath of the MgB_2 conductor, several new strands were designed and fabricated with nonmagnetic 260 brass; these brass-clad strands differed by filament count and the composition of the filamentary matrix with each one being more resistive than copper. The highest number of filaments successfully processed in a single restack designed with a brass outer sheath was 54. AC loss modeling estimated that designing a high filament count MgB_2 conductor with a nonmagnetic filamentary matrix would reduce transport losses by a factor of 10.

Transport losses are clearly influenced by the AC current in the superconductor. The required flux density in the design of the stator coil will determine the wire size based on superconductor current density properties. For example, parameters received from NASA for the 1-MW demonstrator included an operating temperature of 25 K, a maximum applied field amplitude of 0.6 T, with an operating current, I_{op}, of 100 A and safety margin (I_{op}/I_c) of 50%. Based on Hyper Tech's wire performance of 2300 A/mm^2 at 25 K, 0.6 T, the MgB_2 conductor would have to be sized to 1-mm OD to reach an I_c of 200 A. Our AC loss modeling showed that decreasing the safety margin from 0.7 to 0.5 lowered transfer losses by a factor of 3.3 since losses go as the cube of I. Fully transposed multistrand superconducting cables or braids would also decrease transfer losses, since the diameter of the wire is reduced. For example, an MgB_2 wire sized to 0.3 mm in a 10-strand cable would have one-tenth the transfer current loss than that of a 0.96-mm single-strand wire.

Total AC losses. In estimating AC losses, one needs to recognize that loss components are inter-related and various assumptions are made. An example of total loss of a MgB_2 that can be manufactured with good superconductivity properties, a 114-filament MgB_2, comprising of a Cu30Ni matrix (20% cross sectional area), Cu30Ni outer sheath (35%), Nb barrier (33%) and superconductor fraction, λ, of 12%, was estimated in the project based on NASA specifications for the stator coils in the 1-MW demonstrator (at a lower applied field) is listed in Table 4.1.

4.4 Target Markets

This SBIR project demonstrated the manufacturing of low AC loss MgB_2 wires designed not only for motor and generator stator coils, but also for commercial utility transformers and resistive fault current limiters. Hyper Tech continues to market MgB_2 wire technology into several value-added superconducting system businesses. Hyper Tech MgB_2 superconductor wire is the platform technology that is enabling the advancement of several important applications or products including:

1) Helium shortages jeopardize the MRI industry's 10 to 15% annual growth, presently a $4 to $5 billion/year industry. MgB_2 superconductor wire and coils are being developed for helium-free magnets in partnership with manufacturers of MRI devices. MgB_2 wire technology also has a potential market for specialty MRI systems. Hyper Tech currently has a grant to build and demonstrate a background magnet for an image-guided radiation therapy system.
2) MgB_2 wire and coils have been made for both superconducting resistive and inductive fault current limiters. For the utility industry and the Smart Grid, there is the need for new effective tools to limit the growing levels of fault currents that are already developing on the grid due to age and the increasing levels of fault currents arising from distributed energy. This new fault current limiter product area will be a $2 to 3 billion/year market by 2020.
3) The wind industry needs to expand to larger wind systems for land and offshore in order to reduce the cost of energy and reduce their dependence on subsidies. Superconducting generators are the only technology being discussed that can reduce the weight and size of the generators in the 5- to 20-MW range. The development of these low AC loss

MgB_2 wires can enable all cryogenic superconducting wind turbine generators. All cryogenic 10-MW wind turbine generators can reduce the weight and size from 300 to 350 tons to 50 to 70 tons. MgB_2 superconductor wire offers the potential price point, volume of manufacturing, temperature margin, and conductor lengths to meet the needs in the time frames that are required. The projected market for these large wind turbine systems over 10 MW is over a $15 billion/year average in the 2017 to 2030 timeframe.

4) The all-electric, all-cryogenic aircraft market will develop over the 2018 to 2030 time period. This billion-plus dollar market will be enabled by low AC loss MgB_2 superconductors. There will be a huge market for superconducting wire, coils, and systems from the aircraft industry, and additionally for ships and trains.
5) The superconducting transformer market for 60+ MVA transformers can also be a several hundred million dollars per year business. This fine filament low AC loss wire can be directly applicable to the 50 to 60 Hz transformer market.

4.5 Applications

All-electric, all-cryogenic motors and generators using superconductor technology, including magnesium diboride, is of interest for the commercial aircraft industry. Presently major manufacturers of open and closed MRIs, transformers, motors, generators, DC transmission cables, and fault current limiters are pursuing MgB_2 superconductor wires to increase the efficiency and decrease the size of their systems in order to reduce costs. More recently there has been a growing global market for a new class of large machines requiring high power density (from 5 to 20 MW) including wind and wave turbine generators, aircraft turbo-generators, offshore oil platform motors, marine propulsion and generation systems and portable emergency power systems. MgB_2 wires can also be considered or other magnet applications such as magnetic bearings, actuators, magnetohydrodynamic generator (MHD) magnets, propulsion engines, adiabatic demagnetization refrigerators (ADR) coils, magnetic shielding in space, and magnetic launch devices.

4.6 Conclusions

Advances in the development of low AC loss MgB_2 superconductor realized from the NASA SBIR contract increases the TRL for developing all electric aircraft systems. Presently MgB_2 superconductor wire manufactured by Hyper Tech can offer the right combination of properties in the time needed for demonstration in NASA test bed systems, and full size aircraft system implementation in 2020 to 2030 timeframe. Hyper Tech has the technology to specifically tailor the low AC loss MgB_2 conductor design to the engineering requirements of the superconducting stator coils envisioned by NASA.

4.7 Acknowledgments

Jeff Trudell and Gerald Brown of NASA Glenn Research Center for technical guidance and research support, especially during the SBIR project.

4.8 References

4.1 Luongo, Cesar A., et al.: Next Generation More-Electric Aircraft: A Potential Application for HTS Superconductors. IEEE Trans. Appl. Supercond., vol. 19, 2009, pp. 1055–1068.
4.2 Brown, Gerald V.: Weights and Efficiencies of Electric Components of a Turboelectric Aircraft Propulsion System. AIAA–2011–225, 2011.
4.3 Li, G.Z., et al.: Enhanced Higher Temperature (20–30 K) Transport Properties and Irreversibility Field in Nano-Dy_2O_3 Doped Advanced Internal Mg Infiltration Processed MgB_2 Composites. Appl. Phys. Lett., vol. 105, 2014, pp. 112603–1—112603–4.
4.4 Majoros, M., et al.: AC Losses in MgB_2 Multifilamentary Strands With Magnetic and Non-Magnetic Sheath Materials. IEEE Trans. Appl. Supercond., vol. 19, 2009, pp. 3106–3109.

Chapter 5—A Formal Approach to Human-Machine Interaction Analysis Using the Hybrid System Theory

Bong-Jun Yang and Sang Gyun Park
Optimal Synthesis Inc.
Los Altos, California 94022

Inseok Hwang
Purdue University
West Lafayette, Indiana 47907

5.1 Introduction

As modern aircraft cockpit technologies become more complex and rely more heavily on automation, appropriate frameworks for ensuring appropriate human-machine interactions (HMIs) have become an important technical issue for future human-centered automations. In aviation, the development of flight-deck technologies that ensure pilot awareness and appropriate engagement is a central element for ensuring aviation safety under National Aeronautics and Space Administration (NASA) research programs for Next Generation Air Transportation System (NextGen) technologies. Air traffic control (ATC) procedures conceived in the NextGen operations involve automated exchange of information, intent, and instruction among aircraft and between aircraft and the ground. In accordance, the flight deck is expected to rely more on autonomous navigation and control systems, such as a flight management system (FMS). While automation in current navigation and control systems has relieved pilots of repetitive operation of control devices, it has also raised new issues concerning HMIs because the pilot cannot remember all the details of complex automation logics, and dysfunctional interaction between the pilot and the automation can occur (Ref. 5.1).

One of those issues is the lack of awareness for the automation behavior called automation surprises or mode confusion. Mode confusion and other distractions appear to be major causes for pilots to lose situational awareness in many Federal Aviation Administration (FAA) Aviation Safety Reporting System (ASRS) reports and other incidents. The incidents and accidents caused by mode confusion have been studied and are well documented. For example, FAA ASRS reports find that 184 incidents can be attributed to mode awareness problems among considered cases (Ref. 5.2). According to the survey of 1,268 pilots published in 1999 by the Australian Bureau of Air Safety Investigation (BASI), 73% of the respondents indicated that they had inadvertently selected a wrong mode. Moreover, 61% of the respondents agreed that they were still worried about the automation that took them by surprise (Ref. 5.3). Literature surveys reveal that this is a global problem, is prevalent in several types of production aircraft, and occurs in critical phases of flight, especially during takeoff and landing.

The problem of mode confusion can arise due to many reasons, such as complex logics incorporated in the automation, human factors associated with lack of awareness, and poorly-represented or under-represented information on a user interface (UI) to name a few. Mode confusion is typically defined as the discrepancy between the actual state of automation and the state of the pilots' mental mode regarding the automation. Because the problem directly involves human cognition, research on mode confusion has traditionally been addressed from the perspective of engineering psychology. In particular, since the UI is the gateway in which the pilot interacts with the automation, the features of a UI that can lead to mode confusion have been mainly analyzed in those studies. The research on UI characteristics has recently reported findings that human aspects of design such as graphical appearance, layout, and effective ways for alerting should be handled by relying on human cognition and engineering psychology, the information content on UIs can be analyzed under a formal mathematical framework (Refs. 5.4 to 5.6).

This chapter describes the collaborative research on UI validation in terms of HMI analysis, which was performed by Optimal Synthesis Inc. and Purdue University under the support of NASA Langley Research Center.

5.2 Identification and Significance of the Innovation

The technical approach followed in this chapter is in line with those formal mathematical approaches. The hybrid system theory is employed to characterize human operations and automation algorithms in order to investigate the following HMI aspects: (a) whether the information displayed on a UI is sufficient for the pilot to know the flight status and (b) whether a mismatch can exist between the operational mode conceived by a human operator and the actual mode active in the automation. This type of study has been carried out extensively under formal methods.

The approach in this chapter is described by Nandiganahalli, et al. (Ref. 5.7) and has the following features that are different from previous formal methods. Firstly, while most formal methods employ finite-state machine (FSM) models for describing automation logics and human operations, the automation is abstracted as a hybrid system consisting of flight modes and mode-dependent continuous dynamics.

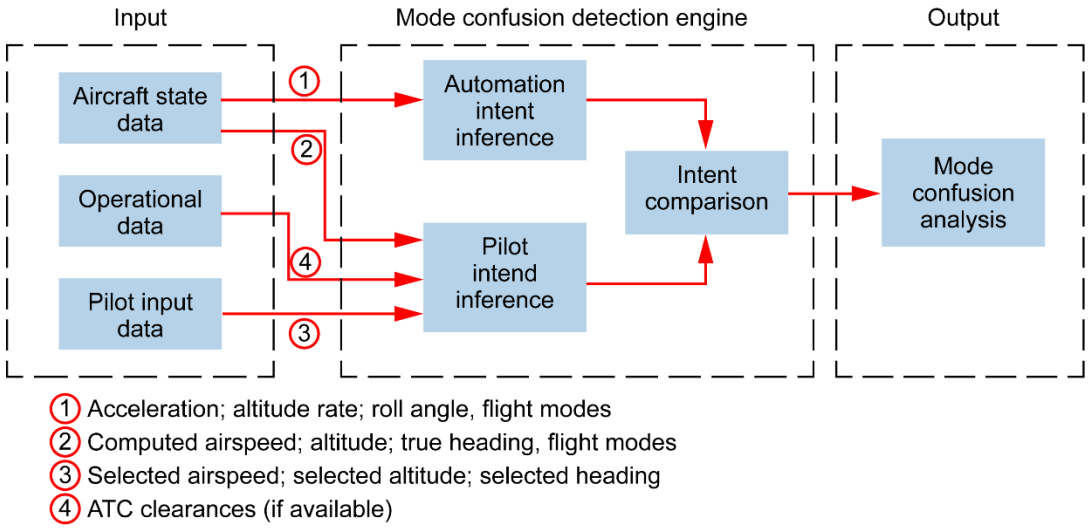

Figure 5.1.—Functional architecture for mode confusion detection tool.

In particular, for mode-confusion detection, a hybrid system whose discrete states include the fight intent instead of traditional fight mode is employed. As illustrated in Reference 5.8, this intent-based abstraction can avoid the state explosion problem typical in logic-based formal methods in dealing with hybrid systems.

Secondly, the notion of the hybrid system allows for the transition among discrete states to be dependent on both continuous states and discrete actions (such as button-push by pilots). As a result, it is possible to characterize more precisely mode transitions occurring in the automation and hence its effect on HMIs.

Thirdly, the approach is data-driven in the sense that it analyzes the simulation or flight data and detects any incident associated with mode confusion. In other words, the approach requires data for analyzing the HMIs under the assumption that a specific UI is already employed. While this limits the use of the approach to the validation of predesigned UIs, it also opens a door to detecting mode confusion incidents that occur due to dynamic interactions between pilots and automations. More specifically, for detecting mode confusion, the approach estimates the intents of the pilot and the automation, in which the intent of the pilot is estimated from the pilots input, the automation status, and operating conditions. This allows for detecting mode confusion when the pilot does not behave as specified in a user manual. In contrast, the previous formal methods logically check whether the requirements for UI has any errors when the user behaves as dictated in a user manual. As a result, the previous formal methods have been restricted to the formal verification of UI specifications in the design phase and hence could not be applied to UI validation. This means that the approach in this chapter is complementary with the previous formal methods.

Finally, the approach is based on the hybrid estimation theory and can be applied to both off-line and online detection of mode confusion incidents. The main difference between them is the type of data, live stream or online data, used for mode-confusion detection.

5.3 Technical Concept and Development

Mode confusion typically happens when the pilot's expected behavior for the automation is different from the actual behavior of the aircraft. In our effort, the notion of behavior is captured by considering flight intents in the speed, vertical, and lateral channels. The flight intent is defined as an element of the flight intent set consisting of 3-tuples as $I = \{I^1, I^2, \ldots, I^{27}\}$ where $I^i = (I_S^i, I_V^i, I_L^i)$ in which $i = 1, \ldots, 27$, and

$$I_S^i \in \{Accelerate, Decelerate, Constant\ Speed\},$$
$$I_V^i \in \{Climb, Descent, Constant\ Altitude\}$$
$$I_L^i \in \{Turn\ Left, Turn\ Right, Constant\ Heading\}.$$

The above equation indicates that the speed intent of an aircraft is abstracted according to its time rate into > 0 (*Accelerated*), < 0 (*Decelerate*), and = 0 (*Constant Speed*). The vertical and lateral intents are determined likewise. That is, the behavior of an aircraft is abstracted using the sign of the time rates of the airspeed, the altitude, and the heading angle. This encapsulates the tactical behavior of an aircraft and characterizes the aircraft behavior at a level higher than the autopilot modes employed for controlling the aircraft. Figure 5.1 shows the functional architecture for the mode-confusion detection tool (MCDT). Since the autopilot logics are typically proprietary in commercial flight control systems, the MCDT is developed such that its reliance on autopilot logics can be minimized.

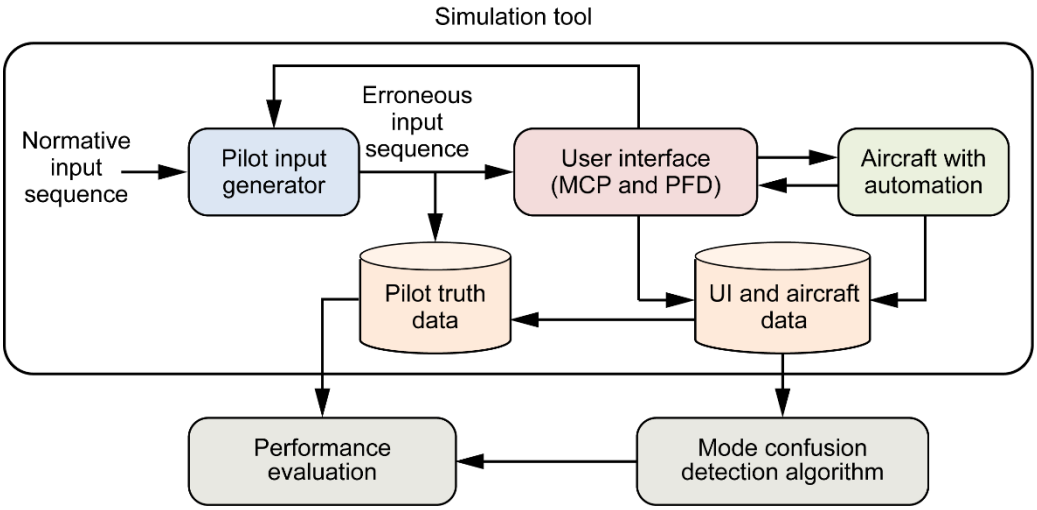

Figure 5.2.—Simulation concept for evaluating mode confusion detection algorithms.

The evaluation of the mode confusion detection algorithm requires a large amount of data in which various types of mode confusion are included. Exhaustive human-in-the-loop simulation can generate such a data, however, associated time and cost is prohibitive because real mode confusion incidents occurring in safety-critical events, such as the one in Asiana accident (Ref. 5.9), rarely happen and are difficult to simulate. In our effort, the scarcity of mode confusion events are overcome by generating pilot inputs based on the human error template (Ref. 5.10). Figure 5.2 shows the simulation diagram employed to simulate mode-confusion incidents in our effort.

The pilot interacts as a supervisor and an observer with the automation, "Aircraft with automation," via the UI consisting of mode control panel (MCP) and primary flight display (PFD). The rationale for the simulation environment is that pilot behavior under degraded situational awareness or human cognition errors is manifested via an aircraft behavior. The inputs on the UI exerted by the pilot, the UI information content, and the aircraft states are saved as "UI and aircraft data." This data is used by the mode confusion detection algorithm, and detected mode-confusion incidents can be compared with "Pilot truth data" for performance evaluation, such as investigating the rates for false detections and missed detections.

For the application of the MCDT, a web-based user interface has been developed. After the MCDT is applied to each individual flight, the detected mode-confusion events can be displayed as shown in Figure 5.3(a) in which Google Map is used for display lateral flight trajectories. The red dots denote the start of the mode-confusion detection and the green dots denote the end of the mode-confusion detection. When the red or green dots are clicked, a new display pops up and shows the intents of the pilot and the automation in the channel of mode confusion as shown in Figure 5.3.

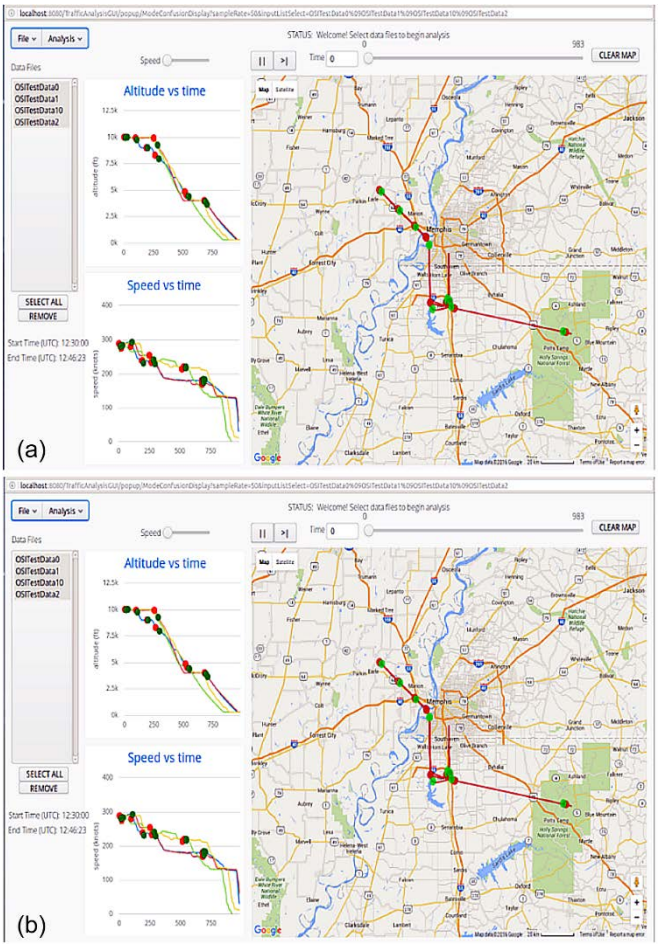

Figure 5.3.—Web-based-developed user interface for mode-confusion detection tool. (a) Display for mode confusion incidents. (b) Display for pilot intent and automation intent. (Map data ©2016 Google)

5.4 Target Markets

The developed software tool is initially targeted for government programs, advanced flight-deck technology development branches of avionics companies, and research institutions. As the recent Asiana accident indicates, human factors and associated cognitive mismatches between automation and pilots are a major contributing factor in transport aircraft accidents. Therefore, ensuring appropriate HMI is a major issue being tackled by aviation safety-related research on flight-deck operations both in government agencies, such as NASA and the FAA, and avionics providers such as Rockwell Collins, Honeywell, Thales, and Garmin and airplane manufacturers such as Boeing, Airbus, and Gulfstream.

In addition, based on recent advances in electronics and computers, new forms of interaction devices—such as larger displays with touchscreen capability, speech-recognition systems, and synthetic vision—are emerging as new technologies, and the developed tool will be a valuable means for analyzing multimodal HMIs. The tool can also be utilized for analyzing HMIs in unmanned aircraft systems.

5.5 Applications

The MCDT tool was applied to a NASA Langley data, and Figure 5.4 shows the altitude and the target altitude in one of the cases in which mode confusion was detected by the MCDT. The detected intent mismatch is shown as the red ellipse. The aircraft begins its initial approach phase starting at 10,000 ft. Between 550 and 682 sec, the aircraft maintains its altitude at 4,000 ft after which it continues to perform the final approach and land at 950 sec. The MCDT detects an intent mismatch when the aircraft transitions from *Constant Atltitude*, that is, level off at the possible minimum decision altitude, to *Descent* at 682 sec. This intent mismatch lasts until 692 sec. at which the selected altitude changes accordingly. During this intent-mismatch period, the autopilot is connected and all the autopilot modes in the vertical channel, for example, VNAV, V/S, FLCH, are disengaged.

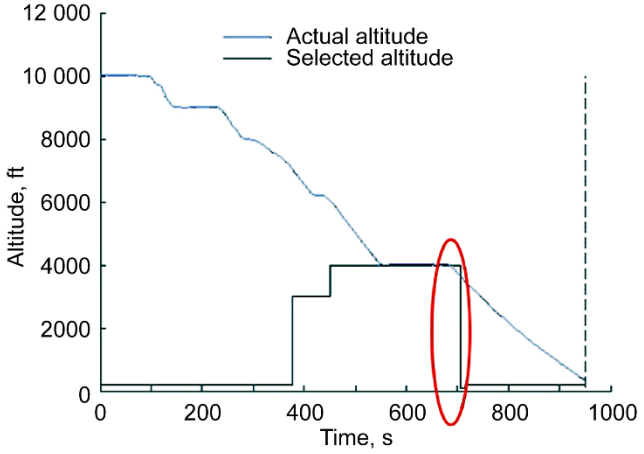

Figure 5.4.—Time histories for actual and target altitudes in NASA Langley data.

5.6 Conclusion

This chapter presents the SBIR effort for detecting mode-confusion incidents that can occur as part of human-machine interactions in modern airplanes. The research consists of implementing mode-confusion detection algorithms together with its Web-based user interface, simulating mode-confusion incidents, and applying the developed prototype to a high-fidelity human-in-the-loop simulation data. The overall research shows that the mode-confusion detection tool can be used to validate a given user interface by finding events that occur in human-in-the-loop simulation or real flights in which anomalous human-machine interactions are detected. These events can occur either due to flaws in the user interface or degraded situation awareness of pilots.

5.7 Acknowledgments

The research was supported under the NASA SBIR Phase II Contract No. NNX14CL15C. Dr. Steven D. Young was the technical monitor. The authors sincerely thank Dr. Young for providing the data and feedback on the development of the pilot input generator and the mode-confusion detection tool. The discussion with him was a major contributing factor for the research described in this chapter.

5.8 References

5.1 Lee, John D.; and See, Katrina A.: Trust in Automation: Designing for Appropriate Reliance. Hum. Factors, vol. 46, no. 1, 2004, pp. 50–80.

5.2 Vakil, Sanjay S.; and Hansman, Jr., R.J.: Approaches to Mitigating Complexity-Driven Issues in Commercial Autoflight Systems. Reliab. Eng. Syst. Safe., vol. 75, 2002, pp. 133–145.

5.3 Bureau of Air Safety Investigation: Advanced Technology Aircraft Safety Survey Report. Department of Transport and Regional Development Report, 1999.

5.4 Degani, A.; and Heymann, M.: Formal Verification of Human-Automation Interaction. Hum. Factors, vol. 44, no. 1, 2002, pp. 28–43.

5.5 Butler, R., et al.: A Formal Methods Approach to the Analysis of Mode Confusion. Proceedings of the AIAA/IEEE/SAE Digital Avionics Systems Conference, Bellevue, WA, 1998.

5.6 Leveson, N., et al.: Analyzing Software Specifications for Mode Confusion Potential. Proceedings of a Workshop on Human Error and System Development, Glasgow, Scotland, 1997, pp. 132–146.

5.7 Nandiganahalli, Jayaprakash Suraj, et al.: User Interface Validation Using Mode Confusion Detection. AIAA 2014–2349, 2014.

5.8 Nandiganahalli, Jayaprakash Suraj, et al.: Intent-Based Abstraction for Formal Verification of Flight Deck Mode Confusion. AIAA 2016–0129, 2016.

5.9 National Transportation Safety Board: Descent Below Visual Glidepath and Impact With Seawall, Asiana Airlines Flight 214, Boeing 777-200ER, HL7742. Technical Report NTSB/AAR–14/01, PB2014–105984, 2014.

5.10 Stanton, N.A., et al.: Predicting Design Induced Pilot Error in the Cockpit. JAAA, vol. 42, no. 1, 2010, pp. 1–10.

Chapter 6—Novel Method of Plasma Flow Control for Drag Reduction

Christopher C. Nelson, Alan B. Cain, and Mehul P. Patel
Innovative Technology Applications Company, LLC
Chesterfield, Missouri 63006

Flint O. Thomas and Thomas C. Corke
University of Notre Dame
South Bend, Indiana 46556

6.1 Introduction

Fuel cost is the largest contributor to commercial airplane related operating cost at up to 50 and 60% for single and dual aisle aircraft, respectively. Similarly, the United States Department of Defense is the largest single consumer of fuel in the world with jet fuel accounting for 71% of the military's fuel consumption. This comes as a consequence of the need for the rapid and agile deployment of forces around the globe. It is not surprising then that improving fuel efficiency is an ongoing goal for both government and private industry, within the United States and internationally. Improved efficiency translates not only to reduced operating costs but also to the reduction of greenhouse gas emissions. This is especially important in aircraft operations since the emissions go directly into the upper troposphere. Government regulators and industry associations have set aggressive goals for reducing these emissions, but that will require the development of significant new technologies. In particular, an effective aerodynamic drag-reducing technique would directly assist in reducing fuel consumption, hence reduce fuel expenses and greenhouse gas emissions.

6.2 Identification and Significance of the Innovation

In a recent Phase I SBIR contract sponsored by NASA Langley Research Center, Innovative Technology Applications Company (ITAC), LLC, and researchers at the University of Notre Dame developed a new drag-reduction device that has demonstrated unprecedented levels of friction drag reduction – up to 70% in initial wind tunnel experiments. Perhaps most significant, is the finding that the power savings provided by the device exceeds the power input required to operate the actuator. The achievement of drag reduction with net power savings represents a major breakthrough in aerodynamic drag-reduction technology. The technology used to accomplish this is called SLIPPS (smart longitudinal instability prevention via plasma surface), and makes use of a novel, flush surface-mounted plasma actuator.

6.3 Technical Concept and Development

Friction drag results as a consequence of the chaotic turbulent flow over an aerodynamic body like a wing or fuselage. If the turbulence could be reduced or eliminated, so too would the associated friction drag and fuel savings be realized. Previous work has demonstrated that turbulent flow over aerodynamic surfaces results from an instability of relatively low-speed streamwise streaks that are located very near the surface. This instability is called streak transient growth (STG) and is associated with the lift up of these streaks from the surface. Once the streaks begin to lift away from the surface, they very rapidly undergo instability and subsequent breakdown to yield turbulent flow. It follows that if the lift-up of low-speed near-wall streaks could be prevented, this would inhibit STG and thereby intervene in the self-sustaining mechanism of turbulence production.

The SLIPPS actuator is a flush, surface-mounted pulsed-DC plasma actuator. This device consists of an array of surface electrodes on the aerodynamic surface that are oriented in the streamwise direction. These are flush mounted to a dielectric material. Beneath the dielectric material is an array of covered electrodes. A common DC source is fed to both the covered and exposed electrodes. A fast-acting, solid-state switch periodically shorts the voltage fed to the lower electrode to the power supply ground. This gives rise to the creation of weakly-ionized plasma near the aerodynamic surface. In the SLIPPS actuator this creates a plasma-induced spanwise-oriented flow near the wall that serves to flatten the low-speed streaks and prevent their lift up. In this manner, the device intervenes in STG and the associated mechanism of turbulence production. Furthermore, the input power required for pulsed-DC plasma actuators in extremely small, which is key in achieving net power savings.

An example of results achieved in wind tunnel experiments at the University of Notre Dame in Figure 6.1 shows the percentage change in friction drag measured on a flat test plate as a function of the number of low-speed streaks under simultaneous control by the SLIPPS actuator. This figure shows that the greatest drag reduction of nearly 70% is associated with the simultaneous control of approximately eight low-speed streaks. As the number of streaks under simultaneous control is increased, the effect of flow control decreases logarithmically. This provides important guidance for the design of SLIPPS drag reduction devices for specific flight regimes.

Based on the Phase I results, a preliminary analysis has been conducted into the scalability of the SLIPPS approach as Mach number increases. If the 60% drag reduction observed in the Phase I effort is consistently attained at higher Mach numbers, these calculations indicate that, for subsonic flows up to at least Mach 0.6, the drag reduction achieved relative to the

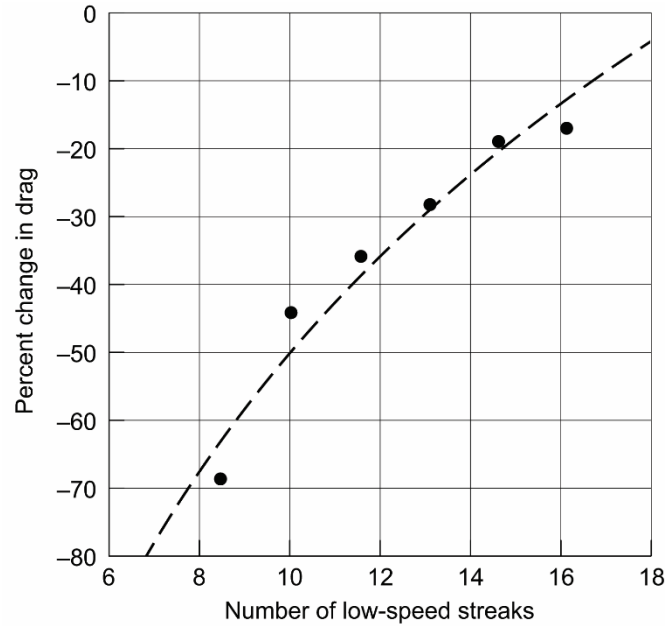

Figure 6.1.—Measured percent change in drag as a function of the number of low-speed streaks under simultaneous control by the SLIPPS actuator.

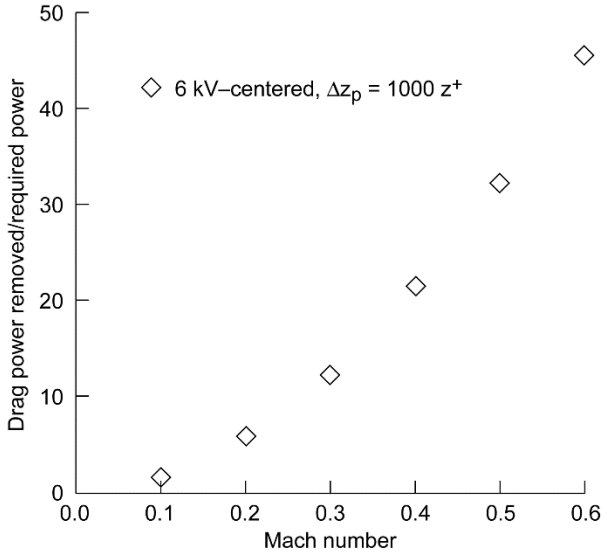

Figure 6.2.—Projected net power savings from SLIPPS as a function of Mach number based on the Phase I results.

required power input into the SLIPPS system improves dramatically as Mach number increases. This is illustrated in Figure 6.2, which shows the ratio of the drag power reduction achieved by a SLIPPS actuator relative to the power required to operate it as a function of Mach number. A similar analysis shows that even if only a 10% drag reduction is achieved throughout the Mach number range, this would still yield a net drag reduction of more than five times the power required to run the SLIPPS system at Mach 0.6. A follow-on Phase II SBIR effort has begun that will provide confirmation of these predictions.

A conceptual design performance analysis indicates that the benefits seen in the lab-scale experiments described above could translate to significant performance improvements for commercial airliners. For an aircraft such as the Boeing 777-300ER, this analysis indicates that SLIPPS could enable a more than 14% increase in range for the same payload. Alternatively, when flying the original range, a greater than 13% payload increase is possible. This level of performance improvement is comparable to (and complements) that offered by the latest engine redesigns from the major engine manufacturers. SLIPPS thus represents the potential for a major competitive advantage for the U.S. aircraft industry if fully developed and broadly adopted.

6.4 Target Markets

The initial markets for production-ready SLIPPS system would be aircraft prime contractors and airframe component manufacturers involved in the building of flight vehicles. Because SLIPPS is a plasma-based technology, vehicles that operate in dry air for long periods at a time have the greatest potential to benefit from the addition of this technology. There are numerous applications which meet this requirement in commercial, military, and general aviation, and we therefore expect interest from a wide range of manufacturers. We also anticipate that aftermarket systems manufacturers would be interested in developing kits to retrofit existing aircraft with SLIPPS systems.

6.5 Applications

Initial applications for a production SLIPPS technology would involve long range and long endurance flight at high altitude. There are numerous applications of this sort in commercial, military, and general aviation. As discussed, SLIPPS offers major benefits for commercial airliners, whether in the form of increased range, increased payload, decreased fuel consumption, or a mix of all three. The same benefits accrue to cargo and transport aircraft of all types.

Preliminary analysis indicates that High Altitude Long Endurance vehicles, both civilian and military, would also benefit greatly from the reduced viscous drag made possible by SLIPPS. The Global Hawk unmanned aerial vehicle (UAV) is an example of this class of aircraft.

Airplanes that fly in dry weather conditions at lower altitudes could also see similar benefits from this technology. SLIPPS offers improved loiter time, reduced fuel consumption, and other benefits for these applications as well. Target vehicles of this sort would include general aviation platforms and small UAVs.

NASA itself operates a number of vehicles which, if retrofit with SLIPPS actuators, could benefit from the resulting reduced viscous drag. This includes the various transport aircraft (e.g., C-5, and NC-130B), drones (e.g., MQ-9), and business jet-

based platforms (e.g., G-II and G-III) used to support NASA's mission.

Because viscous drag has such an important influence on the performance of so many different aerospace systems, the range of potential applications for the SLIPPS approach to drag reduction is extremely extensive.

6.6 Conclusion

SLIPPS technology represents a revolutionary breakthrough in drag reduction. Preliminary versions of this approach have already demonstrated net power benefits for low speed flows, and our analysis indicates that the benefits—drag reduction versus input actuation power—increase substantially as Mach numbers rise (up to at least Mach 0.7, and probably higher). NASA's investment in the development of SLIPPS, in the form of an ongoing Phase II SBIR contract, will allow the ITAC team to verify some predictions from our preliminary analysis and move this important new technology close to flight readiness.

SLIPPS offers significant benefits that advance the objectives of NASA's Advanced Air Transport Technology program. The reduced fuel consumption made possible through dramatic reductions in viscous drag over long flights also complements NASA's Environmentally Responsible Aviation initiative. In addition, SLIPPS supports related government and industry initiatives to reduce greenhouse gas emissions from aircraft.

Chapter 7—Specification Editing and Discovery Assistant for C/C++ Software Development

David R. Cok
GrammaTech, Inc.
Ithaca, New York 14850

7.1 Introduction

The Specification Editing and Discovery project (SPEEDY) produced a tool that augments a modern IDE (Interactive Development Environment), specifically Eclipse, with an editor for formal specifications as part of a C software development environment, advice describing how to work with formal specifications, automated tools that check the consistency of programs and specifications, and tools to discover specifications from source code as an assist to writing them. The overarching goals were to produce a tool that facilitates using formal methods by software engineers, rather than formal methods experts.

7.2 Identification and Significance of the Innovation

Ensuring safety and security in software has been technically difficult since software first began to be produced. The problem is especially acute in domains of interest to NASA such as aerospace, but is a concern for many other domains as well. Some examples are medical devices, industrial control, and control of (perhaps robotic) personal vehicles. The problem motivated the need for sound analysis tools (tools that do not miss flaws) that check and validate software. But building tools that ensure software correctness is challenging—to date no widely-deployable, general solutions have been offered. Thus correctness and safety are obtained only partially, often by applying expensive expert labor.

Using formally specified requirements and automated reasoning tools to check that implementations match requirements is one technology that aids in ensuring software correctness and security. However, adoption of such technologies has been hampered by the lack of tools integrated into the software development environments that are used in day-to-day software development and that can assist software engineers new to formal requirements in writing, editing, reviewing and checking such requirements and the corresponding software.

A clear opportunity is to develop and deploy technologies that enable easy and effective generation, manipulation, and checking of modular formal specifications by software engineers who are not formal methods experts. Two problems must be solved: (a) assembling and integrating an appropriate collection of automated technologies that generate and check specifications, integrated behind the scenes, and (b) doing so in a way that is accessible, even inviting, to most software developers.

7.3 Technical Concept and Development

The technical implementation of the SPEEDY concept required making choices among specification languages, Graphical User Interface (GUI)-based development environments, and technologies for specification assistance, specification checking, and specification inference. The following subsections describe the rationale and resulting choices for each of these subsystems. The SPEEDY project integrated all of these into a productive work environment for software written in the C programming language.

Recall that an overall objective of the project is to make using formal methods a natural part of ordinary software development. In this context, formal methods typically consists of static analysis of software. In static analysis, the software (either source or machine code) is converted to a logical representation, using the semantics of the source or machine language in which the software is encoded. That logical representation is compared, using appropriate reasoning tools, to a logical representation of the software requirements. There are two sorts of requirements to be considered. First, there are the *implicit* requirements of the programming language. The language allows certain operations and disallows others such as dereferencing a null pointer, accessing an array out of bounds, writing through a pointer to read-only memory, or using library calls illegally (e.g., two *free* calls on the same pointer). These requirements can be checked without having to state any functional or policy behaviors. Second, there are *explicit* safety and security policies and functional behavior properties that must be stated using some machine-understandable form and translated into a logical representation that can be compared to the logical representation of the software itself.

The SPEEDY project focused on the means of writing, reviewing, and checking explicit specifications.

7.3.1 Specification Language

Explicit requirements need to be written in some machine-parsable language with clear logical semantics. Some source-programming-language-independent specification languages have been proposed in the past, such as Z (Ref. 7.1) and Alloy (Ref. 7.2). Others can only express low-level keyword-based specifications, such as SAL (Ref. 7.3) and FindBugs (Refs. 7.4 and 7.5). The Checker (Ref. 7.6) tool extends types to provide additional levels of checking.

But to aid adoption we needed a language for which (a) the syntax and semantics are close to the target programming language, (b) expressibility is at least at the level of first-order logic, and (c) there is current experience in the program

verification field. Thus we chose to adopt a programming-language-specific Behavioral Interface Specification Language (BISL) (Ref. 7.7). Many BISLs currently exist: the Java Modeling Language (JML) (Ref. 7.8) for Java programs, SPARK (Ref. 7.9) and the now obsolete ANNA (Ref. 7.10) for Ada programs, Spec# (Ref. 7.11) derived from JML for C# programs, Key (Ref. 7.12), which uses a version of JML for Java Card programs, and Code Contracts (Ref. 7.13) for .NET programs. The corresponding language for ANSI-C is ACSL (Ref. 7.14) (ANSI-C Specification Language), itself derived from JML. All these languages structure specifications similarly: as preconditions (what must be true when a routine is called), postconditions (what is true when a routine terminates), frame conditions (what may change), and invariants (properties of data structures and loops that always hold).

7.3.2 Interactive Development Environment (IDE)

Another project goal was to integrate tools for managing specifications into a common work environment. Because we wanted easy adoption at NASA and elsewhere, we chose an open platform called Eclipse. Eclipse is widely used to build GUI-style IDEs for many different purposes; it has a rich environment for developing Java programs and a younger, but growing, environment for C programs. All the functionality for manipulating C source code is present: editing, compiling, syntax coloring, renaming, refactoring, searching, etc. SPEEDY's task was to extend all of this functionality to act on ACSL specifications as well.

Note that ACSL specifications are expressed as specially formatted programming language comments as shown in Figure 7.1 and Figure 7.2. The result of SPEEDY was to make such specifications full first-class elements within the Eclipse C editor. The specification text is syntax colored; auto-indenting and code completion works in ACSL comments; informational hovers are implemented; key-binding works with any new SPEEDY menu items; parsing and type errors in the

```
5  /*@ assigns \nothing;
6    @ ensures y >= 0 ==> \result <= 0;
7    @ ensures y <= 0 ==> \result >= 0;
8  */
9  int negate(int y) {
10     int j = -y;
11     return j;
12 }
13
14 /*@ requires y != -2147483648;
15     assigns \nothing;
16     ensures y >= 0 ==> \result <=  0;
17   @ ensures y <= 0 ==> \result >= 0;
18 */
19 int negate2(int y) {
20     int j = -y;
21     return j;
22 }
```

Figure 7.1.—Invalid and valid ACSL annotations.

```
4  /*@ ensures 'a' <= c && c <= 'z'
5    @         ==> \result == c - 'a' + 'A';
6    @ ensures 'A' <= c && c <= 'Z'
7    @         ==> \result == c - 'A' + 'a';
8  */
9  int changeCaseBad(int c) {
10     int r;
11     if (c > 'z') {
12         r = c;
13     } else if (c >= 'a') {
14         r = c - ('a' - 'A');
15     } else if (c >= 'Z') {  // Error here
16         r = c;
17     } else if (c >= 'A') {
18         r = c + ('a' - 'A');
19     } else {
20         r = c;
21     }
22     return r;
23 }
```

Figure 7.2.—Text highlights showing counterexample path.

specifications result in Eclipse problem markers; parsing and type checks happen as you type; operations that find declarations and uses of variables or rename variables work across both C code and ACSL annotations; refactoring operations are implemented for annotations just as for C code; Eclipse quick fixes are implemented where appropriate; options are made available in preference and property pages; useful new Eclipse views and an Eclipse perspective for SPEEDY are defined; the structure for internationalization is in place; a special Eclipse console for output related to SPEEDY is implemented; standard Eclipse Help and informational popups provide readily available documentation of ACSL and the SPEEDY functionality.

7.3.3 Programming and Specification Productivity Aids

SPEEDY includes functionality to aid a programmer in writing, editing and reviewing specifications and the corresponding code. In part we followed suggestions from the programming productivity research of the VeriWeb project (Ref. 7.15), in which Ernst and Shiller measured the ability of non-experts to generate and use specifications (for Java) with various user experience enhancements. Their suggestions and the corresponding implementation in SPEEDY are shown in Table 7.1. A key difference is that VeriWeb only considered analysis of dynamic execution traces; SPEEDY also considers static reasoning.

A second important productivity aid is SPEEDY's ability to show counterexample information. When an implementation and the specifications are not consistent, most logical solvers can create a counterexample that shows a concrete case in which the two differ. Understanding counterexamples expressed as models from the solvers themselves is extremely difficult even for experts. The solution prototyped in earlier work (Ref. 7.16) is to (a) translate the counterexample back into source code terms and (b) show the counterexample values directly in the source code editor. A user can readily see the control flow path taken by the counterexample and the values taken by a variable of interest at various points along the

TABLE 7.1.—ADAPTATION OF PROGRAMMER PRODUCTIVITY FEATURES IN SPEEDY

Shiller and Ernst research result	Adaptation to SPEEDY
Drag and drop editing interface	Standard Eclipse editing features: templates, code completion, context assist, keyboard shortcuts
Concrete counterexamples (from execution traces)	Concrete counterexample values and paths, from static analysis, overlaid on the source code implementation
Specification inlining	ACSL specifications are typically written inline in the source code.
Context clues	Suggested locations where specifications should be added
Specification suggestions from Daikon	Specification suggestions from multiple tools, including Daikon (cf. the discussion of Specification Inference in a later subsection)
Active guidance	Active guidance using template-guided editing, code completion, and quick fixes to give suggestions to correct errors; help information available for language features, in context.

execution path. (Note that the analysis is all static, so the 'control-flow path' or 'execution path' is the path that would be taken if the program were executed with the inputs from the given counterexample.) The SPEEDY implementation also allows display by popup windows or hovers of the values of subexpressions within either the code or the specifications. Figure 7.1 shows the result of checking various specifications encoded in ACSL. Valid annotations are colored green and invalid ones read. For an invalid specification, SPEEDY will show the counterexample path that illustrates why the specification cannot be validated: Figure 7.2 shows the path for code that is inconsistent with a postcondition: the path is shown in yellow highlights, with true subexpressions colored green and false ones red.

7.3.4 Specification Checking

It is hard to write correct and complete specifications, just as it is hard to write correct and complete code. Effective tools for debugging both are needed. One such tool is the display of counterexample information described above. That counterexample information comes from logical solvers that compare the implementation and specifications. SPEEDY integrated a number of specification checking tools: the Frama-C weakest-precondition tool, the Frama-C value analysis tools, CpaChecker, and various SMT solvers. The most complete of these for SPEEDY's purpose is the Frama-C WP tool. Though checking using these tools is automated, it is still too time-consuming a computation to perform on-the-fly or even every time a user saves a file. All the implicit and explicit specifications are checked. Success or failure of a check is shown by conventional Eclipse markers. From markers indicating failure, the corresponding control-flow path and concrete counterexample can be obtained. Figure 7.1 shows a simple example: the upper function fails to check (red marker); with an appropriate precondition (the input may not be the minimum representable negative number) the implementation satisfies the specification, as shown in the lower part of Figure 7.1.

7.3.5 Specification Inference

Writing specifications is time consuming; software developers often resist writing them because of unfamiliarity and because it seems like duplicate work. A key element of SPEEDY is to assist in generating first drafts of specifications. One means to do so is to infer a specification from an existing implementation. This is equivalent to code summarization. When successful, it can produce succinct summaries of the code to use as a starting point for editing. The engineer would then review, edit, and embellish the auto-generated summary into a full specification.

Just as for autogenerated tests, autogenerated function summaries must be used with care. Both generated tests and generated specifications will, by definition, agree with the code even if the code is incorrect. Thus they require human review. The goal is that by restating the code's behavior in summary form, any errors in the code will be more obvious and more likely to be identified in human review.

The SPEEDY project integrated a number of existing tools that provided function summaries (CodeSonar®, Frama-C, and Daikon) and also reimplemented algorithms described in academic papers. This aspect – providing specification inference – is the research component of SPEEDY that continues beyond the specific 2-year NASA-funded project. We anticipate publishing a research paper on the success of function summarization in about a year.

There is much literature on procedure and loop summarization, too much to discuss here. There were some interesting observations from this part of our research, such as that (a) many papers deal with special cases of code constructs and need to be placed in a much more general context to be useful and (b) many published reports contain inadequate detail to reimplement or to reproduce the results. Most crucial, however, when we analyzed example code we found that many loops were quite straightforward: they had simple iteration structures and uncomplicated data dependence. This suggested that over half of the loops could be summarized by simple inference algorithms and the resulting loop summaries would provide an immediate benefit for engineers. The final conclusion of that research will be in the research paper mentioned above.

7.4 Target Markets

The target markets include any software development activity for which safety and security are important.

NASA itself develops a great deal of safety and assurance critical software. The historical priorities have included safety of commercial avionics, safety of manned space flight, and correctness of mission control software so that expensive, even

if un-manned, space probes do not fail on their one and only attempt to accomplish a mission. The occasional software failure in the past has led to a discipline of restrictive coding rules (Ref. 7.17) to minimize error and extensive model checking to augment testing (Ref. 7.18). Verification through logical analysis and automated decision procedures provides an additional layer of assurance.

Most of GrammaTech's (GrammaTech, Inc.) market for bug-finding tools is embedded software, that is, applications that control systems that generally run continuously and autonomously. In this application space, upgrades can be infrequent, difficult, and expensive. In addition, the software may be part of cyberphysical systems whose failure can have safety-related consequence. Consequently, the extra effort of writing requirements as machine-readable, logical specifications in order to improve the likelihood of being correct is worth the cost. Furthermore, embedded software applications are typically smaller than average, so problems or costs that may come with large scale applications are less frequent.

7.5 Applications

SPEEDY can be applied in any software development domain, with several use cases. In typical software development, ACSL specifications can be used as an alternate and more succinct way to express properties of an implementation. The tools in SPEEDY can be used to debug the specifications and implementation together. The specifications can also be alternately expressed in more abstract logical terms and thereby related to formal, but more abstractly expressed requirements. The validity of the connections between the code and the more abstract requirements are ensured by automated decision procedures.

In another use case, SPEEDY can be combined with work that first proves that an abstractly conceived and invented algorithm satisfies some important safety property that is complex enough that its validity is not obvious. But then that algorithm needs to be translated into an actual implementation in C code. If the original requirements can be accurately translated into ACSL specifications, then the techniques integrated into SPEEDY can be used to prove the last mile – that the implementation itself is consistent with the requirements.

A third application is to Verification & Validation (V&V) operations. Here the software is received as is, without further development expected. The goal is to independently ensure that the software implements the requirements; if security is also a concern, then the software must also not allow insecure behavior when used in unexpected conditions, such as, with out-of-range inputs. In this use case, the V&V team generates an independent representation of the system requirements as formal specifications and then uses tools such as SPEEDY to ensure, with as much automation as possible, that the implementation is consistent with the requirements.

Finally, formal specifications can be used as checkable documentation. In a review process or reverse engineering endeavor, detailed machine-checkable specifications are used as a way to capture and validate accumulated knowledge of a software system.

7.6 Conclusion

SPEEDY is a NASA-funded SBIR contract that created an environment that aids the writing, editing, checking, inferring, and reviewing logical specifications of ANSI-C code as part of ordinary software development. The tool is implemented as a plug-in to the Eclipse C Development Toolkit. Its uses the ACSL specification language and integrates a number of external tools, such as Frama-C, CodeSonar, CodeSurfer, and Daikon.

7.7 Acknowledgments

The SPEEDY project was supported by NASA SBIR contract # NNX14CL05C (Technical Monitor: Kurt Woodham, NASA Langley). Development of specifications for library routines was in part supported by the NSF: this material is based upon work supported by the National Science Foundation under Grant No. ACI-1314674; any opinions, findings, and conclusions or recommendations expressed in this material are those of the author(s) and do not necessarily reflect the views of the National Science Foundation.

7.8 References

7.1. Spivey, J.M.: The Z Notation: A Reference Manual. Prentice Hall International (UK) Ltd., London, England, 1992.

7.2. Jackson, Daniel: Software Abstractions: Logic, Language, and Analysis. The MIT Press, Cambridge, MA, 2006.

7.3. Using SAL Annotations to Reduce C/C++ Code Defects. http://msdn.microsoft.com/en-us/library/ms182032.aspx Accessed Nov. 7, 2016.

7.4. Cole, Brian, et al.: Improving Your Software Using Static Analysis To Find Bugs. OOPSLA 2006, ACM, New York, NY, 2006, pp. 673–674.

7.5. Pugh, Bill, et al.: FindBugs—Find Bugs in Java Programs. University of Maryland, College Park, MD. http://findbugs.sourceforge.net/ Accessed Nov. 7, 2016.

7.6. Papi, Matthew M., et al.: Practical Pluggable Types for Java. Proceedings of the 2008 International Symposium on Software Testing and Analysis. ACM, New York, NY, 2008.

7.7. Hatcliff, John, et al.: Behavioral Interface Specification Languages. Department of Electrical Engineering and Computer Science Technical Report CS–TR–09–01a, 2010.

7.8. Leavens, G.T., et al.: JML Reference Manual. Iowa State University, Ames, IA, 2007.

7.9. Praxis Critical Systems Limited: A Technical Overview of SPARK. http://www.sparkada.com/overview.html Accessed Nov. 7, 2016.

7.10. Luckham, David C., et al.: ANNA: A Language for Annotating Ada Programs: Reference Manual. Lecture Notes in Computer Science, Vol. 260, Springer-Verlag, Heidelberg, Germany, 1987.
7.11. Barnett, Mike; Leino, Rustan; and Wolfram Schulte: The Spec# Programming System: An Overview. Construction and Analysis of Safe, Secure, and Interoperable Smart Devices, Lecture Notes in Computer Science, Vol. 3362, 2004, pp. 49–69.
7.12. Beckert, Bernhard; Hähnle, Reiner; and Schmitt, Peter H.: Verification of Object-Oriented Software: The KeY Approach. Lecture Notes in Computer Science, Vol. 4334, 2007.
7.13. Fahndrich, Manuel, et al.: Integrating a Set of Contract Checking Tools Into Visual Studio. Proceedings of the 2012 Second Workshop on Developing Tools as Plug-ins, Zurich, Switzerland, 2012.
7.14. Baudin, Patrick, et al.: ACSL: ANSI/ISO C Specification Language. Version 1.4, CEA LIST and INRIA, 2009–2010. http://frama-c.com/download/acsl_1.4.pdf Accessed Nov. 7, 2016.
7.15. Schiller, Todd W.; and Ernst, Michael D.: Reducing the Barriers to Writing Verified Specifications. Proceedings of the ACM International Conference on Object Oriented Programming Systems Languages and Applications, ACM, New York, NY, 2012, pp. 95–112.
7.16. Cok, D.R.: Improved Presentation of Counterexample Information Using Incremental SMT Provers. Verified Software: Theories, Tools and Experiments (VSTTE) Tools Workshop, 2008.
7.17. Holzmann, G.H.: The Power of 10: Rules for Developing Safety-Critical Code. IEEE Computer, vol. 39, no. 6, 2006, pp. 95–99.
7.18. Holzmann, Gerard: The SPIN Model Checker: Primer and Reference Manual. Addison-Wesley Professional, 2003

Chapter 8—Unmanned Aircraft System Safety Analysis Model

Ankit Tyagi and Frederick Wieland
Intelligent Automation Inc.
Rockville, Maryland 20855

Stefan Toussaint
Coherent Technical Services Inc.
Lexington Park, Maryland 20653

James T. Luxhøj
LCR LLC
Somerset, New Jersey 08873

8.1 Introduction

The goal of introducing Unmanned Aircraft Systems (UASs) in the U.S. civilian airspace or National Airspace (NAS) continues to attract government and private researchers. The Federal Aviation Administration (FAA) is bound by the Public law 112-95, Title III, Subtitle B1 of 2012 to work towards integration of civil unmanned aircraft systems into the National Airspace (NAS). In anticipation, other government agencies such as U.S. Department of Homeland Security, Forest Service, and Environmental Protection Agency (Ref. 8.1) have already defined specific UAS missions and possible target areas for their UAS applications. Similarly, private entities such as big box retailers and online suppliers are investing resources to be ready to use UASs as well. Research at Intelligent Automation, Inc. estimates that there can be over 25,000 UAS flights per day in controlled airspace in the United States (Ref. 8.2). UASs are slated to have an enormous impact on the global economy with projection of over 12 billion dollars in direct UAS sales alone by the year 2024 (Ref. 8.3).

However, to realize these civilian applications UASs need to operate seamlessly within the NAS while maintaining or exceeding current safety benchmarks. Operational safety should be the primary concern during this initial phase of UAS introduction to NAS. One of the key challenges identified by the Department of Transportation (DOT) and Federal Aviation Administration (FAA), as per the UAS integration into NAS roadmap is to fully research the considerations in introducing UAS operations for their potential impact on safe operations in NAS (Ref. 8.4). Recent reports indicate that even with limited UAS operations in NAS over the past decade there have been more than 70 UAS crashes (Ref. 8.5), 30% of which were civilian UAS. This chapter outlines a holistic approach to UAS safety analyses. The results are computed using UAS Safety Analysis Model (USAM) that approaches UAS safety from three levels of abstractions (1) NAS-wide level (2) Aircraft level (3) Aircraft system level.

USAM is a modeling and simulation based tool that has been in development over the two years and has been described in detail in References 8.6 and 8.7. Figure 8.1 shows the model architecture in the three layers of abstraction. The tool starts at the system level with simulations of both UAS and manned flights in the NAS using the Kinematic Trajectory Generator (KTG) (Ref. 8.8) encounter model (KEM). KEM identifies all Loss of Separation (LoS) events that occur during the scenario under investigation. Next, the Collision Risk Model (CRM) (Ref. 8.9) provides the probability of a Mid-Air Collision (MAC) for a pair of aircraft for which a Near-MAC had occurred. Finally, the Aviation System Risk Model (ASRM) (Ref. 8.10) assumes a MAC has occurred and provides the most probable causes. It also provides a list of mitigation strategies that would be most effective.

8.2 Identification and Significance of the Innovation

The aviation community lacks a UAS-centric safety analysis tool that can enable them to forecast the safety of UAS operations in the NAS. One of the primary reasons for this deficiency is the absence of an extensive record of UAS operational data, as the primary user of UAS to date has been the military. However, the lack of operational data for UAS can be overcome by using a credible industry-vetted source of demand data for UASs, and realistic UAS aircraft performance data that has been vetted by the manufacturers. Both of these datasets are available to Intelligent Automation Inc. (IAI) through previous NASA projects and are inputs for USAM.

The development of a UAS safety analysis tool should be a high priority for the aviation research community. The lack of such a safety tool hampers and decelerates FAA's effort to safely integrate UASs into the NAS. As of the end of November 2012, FAA had approved 345 Certificates of Waiver or Authorization (COA) to public entities for the operation of UAS in U.S. civil airspace.

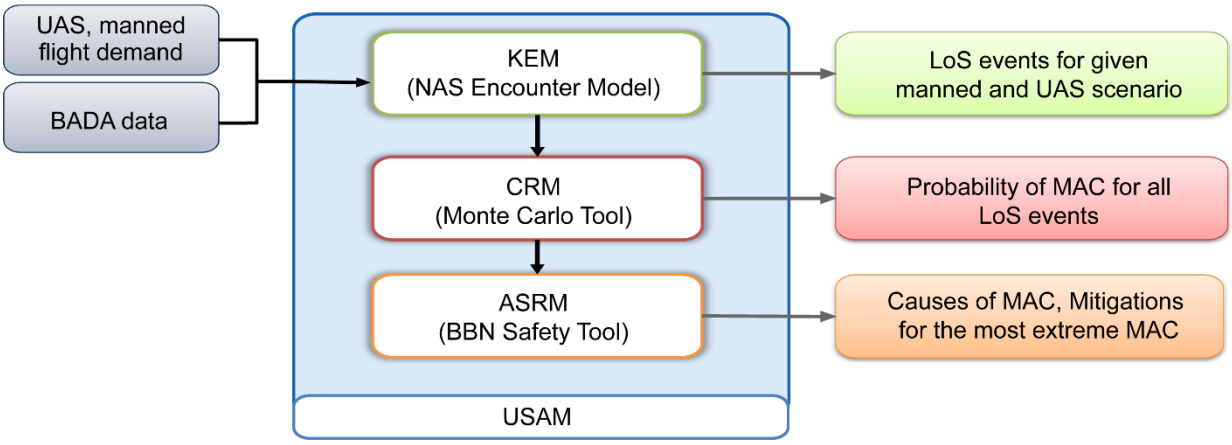

Figure 8.1.—USAM architecture.

However, in order to accommodate the anticipated UAS traffic, the FAA needs to transition to more a routine integration process wherein new or revised operating rules and procedures are put in place and UAS are capable of complying with them (Ref. 8.4). In order to create and modify the operating rules, FAA needs a systematic analysis like USAM.

The rate at which UASs are integrated into the NAS will directly depend on the FAA's ability to create the required operating rules to ensure and maintain the safety of the NAS. Various analysts suggest that Europe, China, and Japan will press ahead with significant UAS development programs. Japan, for example, has already addressed safety and airspace regulatory issues, allowing civilian use of UASs for certain applications, such as aerial spraying of pesticides. Therefore, in order for the U.S. to continue being a leader in global aviation, it needs to facilitate and expedite the process of safe and efficient integration of UASs into the NAS through timely policymaking. We believe that the research proposed here will prove to be a valuable tool that would enable the aviation community and FAA in the timely execution of their mandate.

The aviation research community is only one of the target audiences for USAM. USAM has potential for UAS manufacturers. By producing a software performance model of their proposed aircraft and running the software model in USAM with the simulated commercial traffic, the unique hazards presented by the manufacturer's design can be identified. The manufacturer can then make changes to the design to mitigate these hazards or, if the hazards are improbable enough, go forward with the manufacturing process. Thus, the market for USAM includes, at the minimum, NASA researchers, FAA safety analysts, and UAS aircraft manufacturers.

8.3 Technical Concept and Development

8.3.1 Investigation of Loss of Separation (KEM)

KEM functions in three distinct phases, preprocessing, simulations, and post processing. The model inputs are the UAS and manned performance data in the format of EUROCONTROL's Base of Aircraft Data (BADA) data and flight demand data. IAI has access to 150 BADA manned aircraft data and 14 UAS performance data files. These UAS data files are industry vetted and were developed by IAI as part of a separate study (Ref. 8.11). The flight demand data is also developed by IAI in collaboration with a number of government and commercial entities. The UAS demand data is now available for distribution online (Ref. 8.12). KEM's first phase includes parsing of the flight demand data (Figure 8.2). This data describes detailed flight information like flight Id, aircraft type, cruise altitude, flight path, cruise speed, origin, destination and time of departure. Next phase involves flight simulations using a Kinematic Trajectory Generator.

KEM simulates each flight individually and stores the simulated trajectories in a database. KEM uses an enhanced version KTG that is capable of simulating small UASs in addition to other standard aircraft types. For comparison, results from NASA's Airspace Concept Evaluation System (ACES), a standard modeling and simulation tool reports 8,000 LoS events while KEM reports 10,500 for a standard UAS mission. On average, KEM reports about 1.3 times more LoS events than ACES. This is an expected result since KEM models unimpeded traffic while ACES models Air Traffic Control (ATC) and Traffic Flow Management (TFM) constraints on the flights. Results from KEM flow to CRM for further processing.

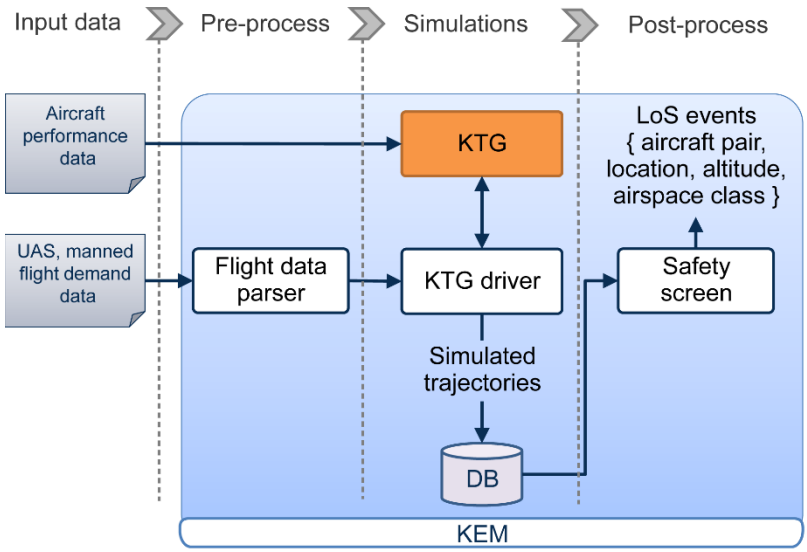

Figure 8.2.—KEM architecture.

8.3.2 Computation of Probability of Mid-Air Collisions Using (CRM)

KEM identifies LoS events between manned flight and UAS for the given UAS scenario. CRM analyzes these events and calculates the probability of a MAC or PMAC for all of them. The most severe PMAC, that is, those aircraft pairs that have the highest chance of collision are assessed in greater detail and finally, the aircraft pair with the highest PMAC is passed on as inputs to ASRM for further processing. Figure 8.3 shows typical results from CRM. Figure 8.3(a) shows the distribution of PMAC values at different values of separation between UAS and manned flight. The P(MAC) increases as the initial separation between the two aircraft decreases and reaches the highest values before reducing again, as the aircraft pass each other. Figure 8.3(b) shows the breakdown of highest PMAC values obtained during a particular UAS mission.

8.3.3 System Risk and Mitigation Estimation

For any safety analysis it is important to identify potential causes of safety violations. These causes may be further classified based on their impact to the overall system safety so that adequate attention may be given to the causes that are most likely to occur or to those that most affect the system safety. The hazard sources can be further broken down in terms of the underlying causal factors—the likelihood assessment of these factors, the severity evaluation of the potential consequences of mishaps, and the prioritization of mitigations. The ASRM is a tool operates on these parameters.

It is a Bayesian Belief Network (BBN)-based tool that starts by identifying the active systems and sub-systems, their interactions, and the causal factors that could trigger and lead to an event. For USAM we use ASRM to investigate the causal factors that could lead to a MAC and the mitigation strategies that would be most effective in avoiding one. Figure 8.4 shows a typical BBN model that consists of nodes. Each node belongs to a particular hazard cluster. Using predefined probabilities of each node's behavior, the entire model can answer prognostic and diagnostic questions. For typical UAS scenarios, we found that communication links in the UAS is the most important node as it has the highest impact on P(MAC) while ATC intervention is the most effective mitigation strategy.

8.4 Target Markets

The FAA is the primary user of USAM since it is a safety analysis tool can perform Operational Safety Assessments to gauge impact of UASs on the system-level safety of the NAS. We also believe that the UAS users can use a tool like USAM for mission planning. USAM could also be used by UAS manufacturers for aircraft design-related guidance. Also, DOD could utilize a tool like USAM to perform mission planning. There is no other tool that can perform such data-driven safety analyses using realistic projections of UAS traffic and manufacturer-vetted UAS aircraft performance data to simulate conflict scenarios. Other companies may develop a safety analysis tool on their own that analyzes a *few* conflict scenarios, but USAM not only produces system-level safety impact of UAS introduction, but also performs a cross-sectional study of specific conflict scenarios that span across different combinations of UAS aircraft and airspace classes.

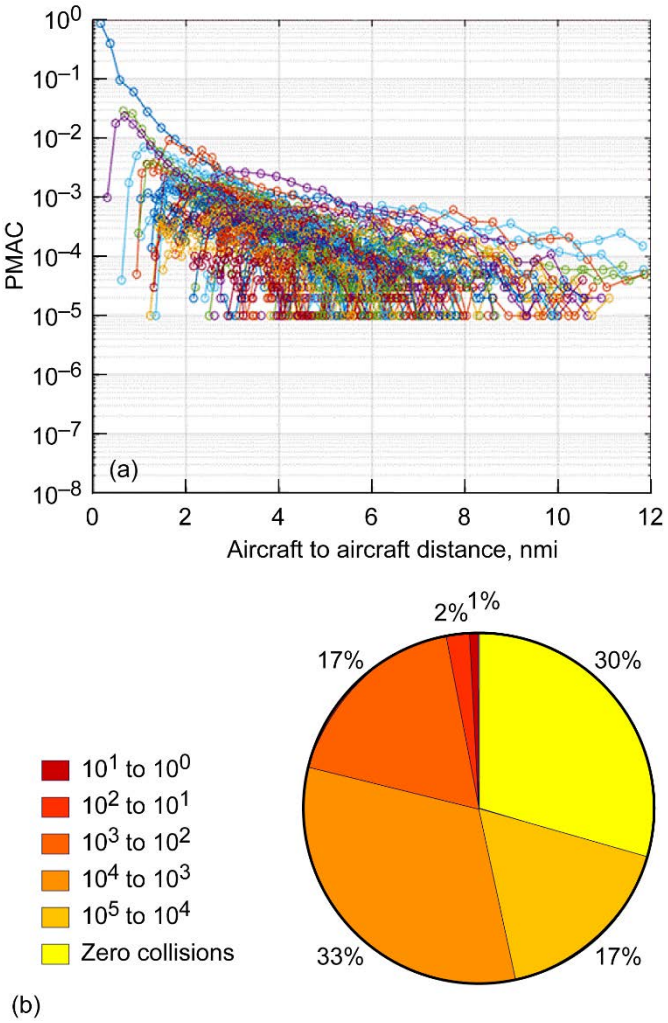

Figure 8.3.—P(MAC) values for (a) all reported LoS events as function of initial aircraft separation (b) LoS and PMAC values.

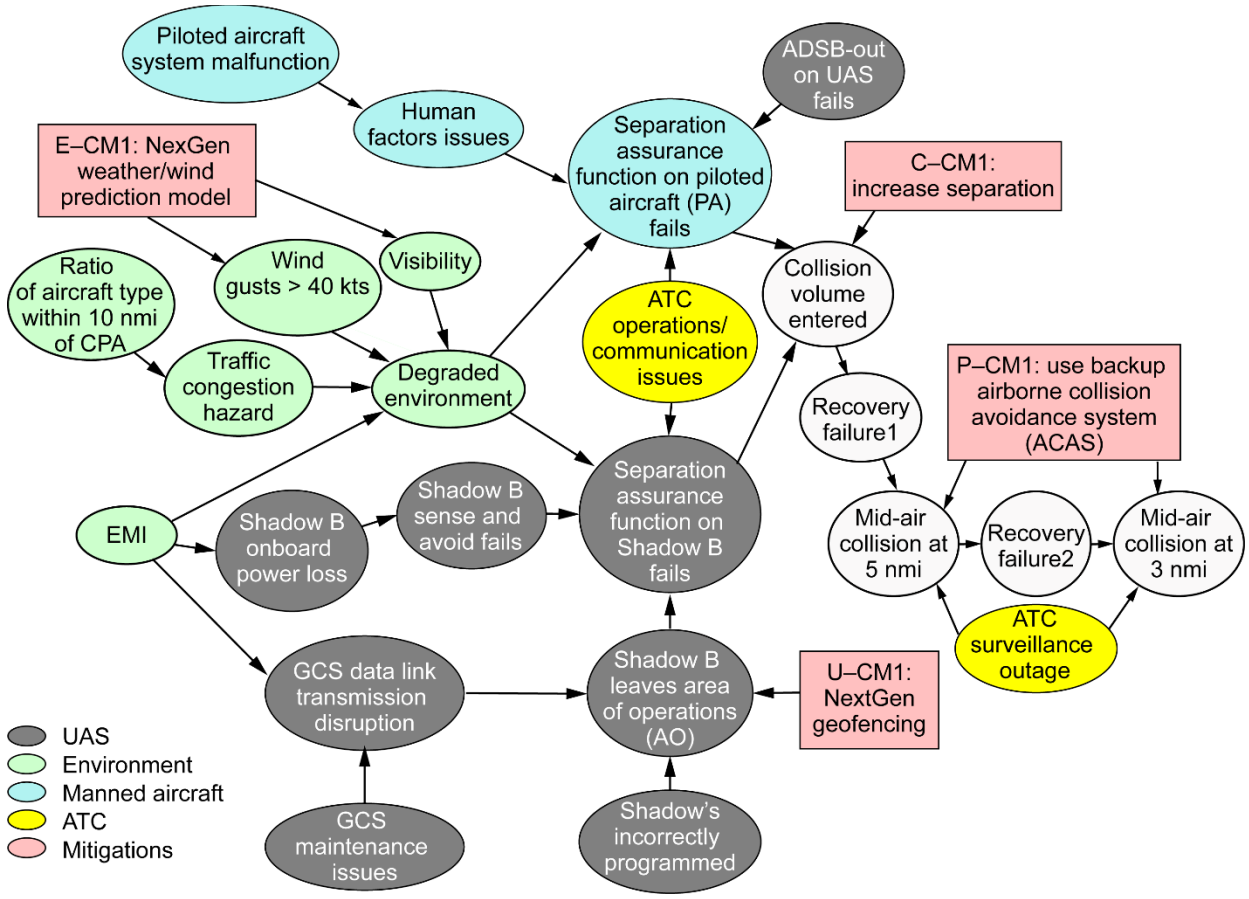

Figure 8.4.—ASRM model for a LoS between a Shadow B UAS and a manned aircraft in Class E Airspace.

8.5 Applications

Results from USAM identify the types of possible safety incidents given a traffic density and UAS mission. They can identify the root cause, down to an aircraft subsystem and identify the best mitigation strategies. These results can provide insights to researchers and regulators and point out shortcomings in existing safety portfolios. Similarly, mitigation options can be compared and contrasted by their effectiveness towards a particular UAS or mission scenario.

8.6 Conclusion

USAM is a mature UAS safety tool designed to investigate UAS integration scenarios at multiple levels of abstraction. The first layer involves an encounter model (KEM) that identifies potential LoS events between a UAS and a manned aircraft. It uses industry-vetted aircraft performance models for both UAS and manned flights. KEM simulates UAS and manned traffic based on flight schedules obtained by governmental agencies. By simulating unimpeded traffic, KEM reports LoS events in far greater number than other modeling tools such as ACES while improving run time significantly. A safety tool's preference is to investigate as many variations of LoS events as possible therefore USAM uses KEM instead of ACES-like tools. Our results indicate KEM reports about twice as many LoSs than ACES and takes half the amount of time to run. With parallel processing and other tweaks, KEM run time can be reduced to a few minutes.

The next USAM abstraction layer operates on NAS-wide LoS events. For each aircraft pair, CRM performs a Monte Carlo analysis by simulating 100,000 trajectories and computing the probability of a MAC occurring. CRM uses a physics-based trajectory generator to simulate these trajectories that use industry standard aircraft performance data. CRM identifies the risks of MACs at a number of locations along the aircraft trajectory to estimate the effectiveness of possible mitigation strategies. It identifies the aircraft pair with highest risk of MAC and initiates transfer to the next USAM layer.

ASRM is a BBN-based risk assessment model that can identify the possible root causes of a MAC. The tool starts with a detailed model of the two aircraft and their safety-critical subsystems as well as the ATC and environmental factors. The probability of failure of each node is sourced from real world data or simulations. ASRM identifies the most probable causes of MACs by comparing the impact each node has on the final outcome. ASRM also compares the effectiveness of mitigation strategies and identifies the one that is most likely to avoid a collision.

8.7 References

8.1. Federal Aviation Administration: Air Traffic Organization Policy. FAA ORDER JO 7110.65W, 2012.

8.2. Wieland, F.: The Drones are Coming: Is the National Airspace System Prepared? Journal of Air Traffic Control, Quarter 2, 2016.

8.3. The Drones Report: Market forecasts, Regulatory Barriers, Top Vendors, and Leading Commercial Applications. Business Insider, 2016. http://www.businessinsider.com/uav-or-commercial-drone-market-forecast-2015-2 Accessed Nov. 7, 2016.

8.4. U.S. Department of Transportation: Integration of Civil Unmanned Aircraft Systems (UAS) in the National Airspace System (NAS) Roadmap. Federal Aviation Administration, Washington, DC, 2013.

8.5. Whitlock, Craig: Close Encounters on Rise as Small Drones Gain in Popularity. Washington Post, Springfield, VA, 2014. http://www.washingtonpost.com/sf/investigative/2014/06/23/close-encounters-with-small-drones-on-rise/ Accessed Nov. 7, 2016.

8.6. Tyagi, Ankit, et al.: Investigation of Simulated UAS Safety Incidents Using UAS Safety Analysis Model (USAM). AIAA 2015–3406, 2015.

8.7. Kumar, Vivek, et al.: UAS (Unmanned Aerial System) Safety Analysis Model (USAM). AIAA 2014–2285, 2014.

8.8. Intelligent Automation, Inc.: Kinematic Trajectory Generator. http://www.i-a-i.com/?product/ktg Accessed May 5, 2016.

8.9. Toussaint, Stefan; and Gallimore, Ian: Collision Risk Model for Navy UCAS ATC Using Cooperative GPS/INS Surveillance. AUVSI Unmanned Systems North America Conference 2009,Washington, DC, 2009.

8.10. Luxhøj, James T.: Probabilistic Causal Analysis for System Safety Risk Assessments in Commercial Air Transport. NASA/CP—2003-212642, 2003. http://ntrs.nasa.gov

8.11. Ayyalasomayajula, Sricharan, et al.: Unmanned Aircraft System Demand Generation and Airspace Performance Impact Prediction. Presented at the 2013 IEEE/AIAA 32nd Digital Avionics Systems Conference, East Syracuse, NY, 2013.

8.12. Intelligent Automation, Inc.: UAS-Max Projection of Future UAS Flights. http://www.i-a-i.com/?product/uas-max Accessed May 5, 2016.

Chapter 9—Raman Icing Detection System

D. Fourguette, L. Jones*, W. Johnson, K. Moncur, and J. Pavlich
Michigan Aerospace Corporation
Ann Arbor, Michigan 48108

9.1 Introduction

Inflight icing of engines and airframes presents a significant hazard to air transport, especially at lower flight elevations during takeoff or on approach. Michigan Aerospace Corporation (MAC) has developed a short-range optical instrument capable of identifying icing conditions while also allowing for air data sensing as well as other hazard detection capabilities. The Raman Icing Detection System (RIDES) is a compact Raman spectrograph designed to collect the Raman-scattered light from the air flow in the free stream of the aircraft. The device operates without protrusions into the flow, behind a flush-mounted window on the skin of the aircraft, mitigating the risk of ice buildup during operation.

9.2 Identification and Significance of the Innovation

Inflight icing of engines and airframes presents a significant hazard to air transport, especially at lower flight elevations, on approach. Ice accretions on the wings affect the smooth flow required for proper lift. A thin layer of coarse ice can reduce the lift by 30% and increase drag by up to 40%. In addition, accretions can also reduce the air intake in engines and affect readings from a (heated) Pitot tube. Freezing rain and drizzle, often found in wet clouds, represent the most dangerous conditions for icing. Super-cooled large droplets (SLDs) freeze upon impact with a cold surface (such as a wing) and rapidly distort airfoil shapes, affecting the air flow and the lift. Icing conditions often appear suddenly for a given aircraft. Ideally, pilots would have a cockpit display of the icing conditions up ahead in order to make educated decisions on the flight path (Ref. 9.1).

The RIDES technology developed under this NASA-funded SBIR effort included the design, fabrication, assembly, and testing of a short-range Raman-based optical sensor to determine the water phase composition ahead of the aircraft. At the core of the RIDES development is a custom spectrograph specifically designed to resolve the Raman spectrum of water and nitrogen. RIDES is designed to operate in conjunction with an optical air data sensor (OADS), also developed by MAC. This optical air data sensor measures airspeed, temperature, and density outside the aircraft boundary layer. The two instruments share the laser and receiver; a filter assembly separates the collected light into two components. The elastically-scattered light is directed to the air data sensor while the Raman contribution, at longer wavelengths, is sent to the RIDES spectrograph. The optical instrument operates in the solar-blind region of the spectrum.

9.3 Technical Concept and Development

Raman scattering has been successfully demonstrated to determine the relative concentration of water in three phases in dry and rainy atmospheric conditions (Ref. 9.2). Using 1-nm resolution, Park et al. (Ref. 9.2) showed that the Raman spectrum (using a triple Nd:YAG (neodymium-doped yttrium aluminum garnet) laser as its light source, 354.7 nm excitation wavelength) exhibits features between 400 and 410 nm depending on the relative concentration of the three phases. The first step in the instrumentation development was the calculation of the water Raman spectrum in the OH stretching region. Figure 9.1 shows the Raman spectrum for the three phases of water. The water vapor spectrum was calculated using the database compiled by Avila et al. (Ref. 9.3) and the liquid water and ice spectra were calculated using Sun and Zheng's approach (Ref. 9.4).

The second step in the instrumentation development was the spectrograph design and fabrication. The RIDES custom spectrograph is shown in Figure 9.2. The light is brought to the spectrograph using a multimode fiber. The input light is collimated before impinging upon the grating. The dispersed light is focused onto a CCD (charge coupled device) array. The spectrograph is calibrated for spectral response using an ultraviolet (UV) light-emitting diode (LED) and the spectrum of a xenon source. The xenon spectrum obtained with the RIDES spectrograph compared well with the same spectral range obtained with a MAYA2000 Pro (Ocean Optics) spectrograph.

After calibration, the spectrograph was integrated into a test setup composed of a quadrupled YAG emitting at 266 nm and a receiver assembly. The backscattered light from air, water, and ice was collected and passed through the RIDES spectrograph. The following results are preliminary but very encouraging. Figure 9.3 shows the Raman spectrum of air, water, and ice combined into one plot. The nitrogen line (shift = 2331 cm^{-1}) is clearly visible at 283.5 nm, and the water and ice spectra show the typical broad Raman line distribution.

The shape and the wavelength at which the liquid water Raman spectrum exhibits a maximum depends on the temperature (Ref. 9.5). A series of measurements with water temperature ranging from 5 to 30 °C was conducted to evaluate

*Currently with Electro-Optics Technology, Inc., Traverse City, MI.

the spectrograph's ability to provide water temperature. Figure 9.4(a) displays the spectral region at maximum signal and Figure 9.4(b) shows the wavelength of the maximum point versus temperature. The maximum was determined using a spline fitting and a maximum-finding algorithm developed in Python software.

These results are preliminary and additional work will be performed to fully characterize the spectrograph and demonstrate the capabilities in the field.

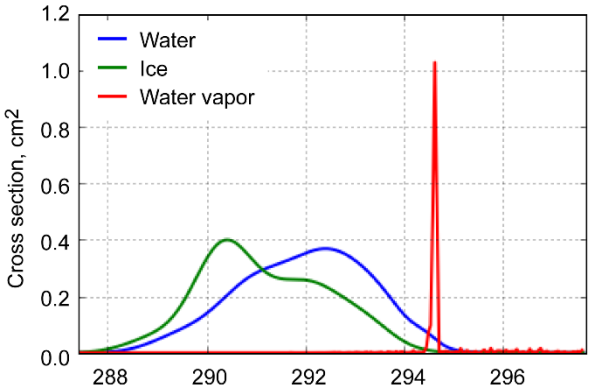

Figure 9.1.—Water Raman spectrum (excitation at 266 nm).

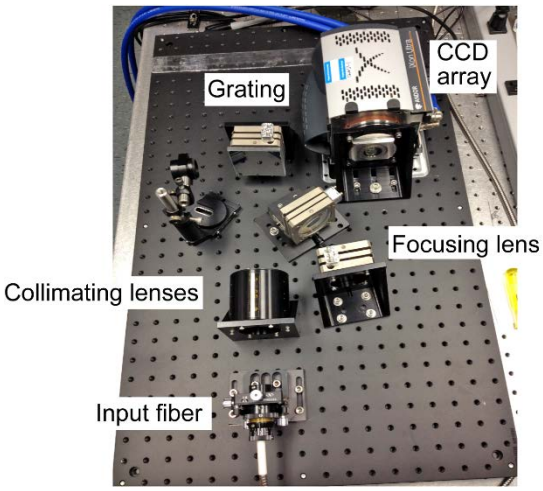

Figure 9.2.—Benchtop RIDES spectrograph.

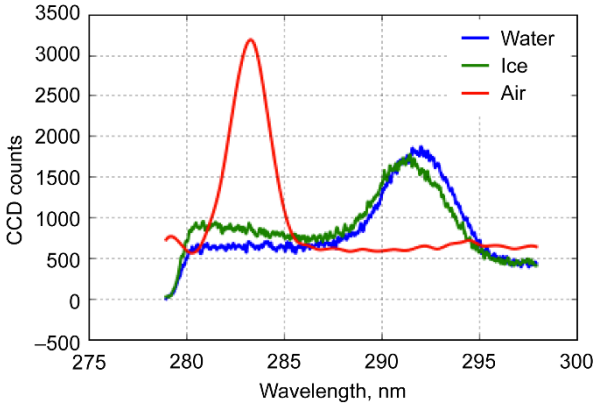

Figure 9.3.—Air showing the combined N_S line (283.5 nm), water, and ice spectra obtained with the RIDES spectrograph.

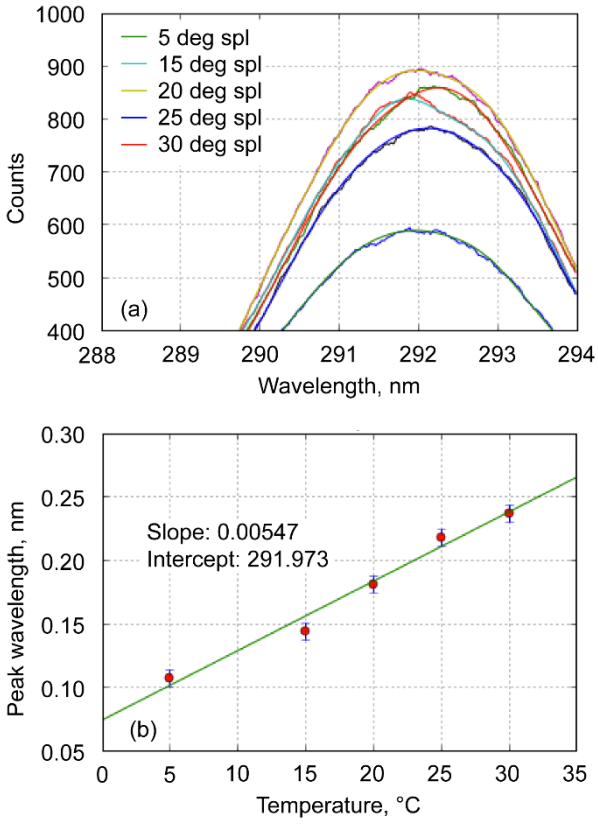

Figure 9.4.—Water spectra at (a) Temperatures ranging from 5 to 30 °C. (b) Spectral dependence on the maximum.

9.4 Target Markets

Military and civil aviation is often affected by icing, sometimes severely (e.g., Comair flight 3272 in 1997, Air France flight 447 in 2009) and the ability to detect these conditions so as to avoid or at least account for them (activating de-icing systems, etc.) would be of tremendous safety value, suggesting a substantial market. MAC is currently developing an OADS. Such an instrument combined with RIDES will provide a powerful suite of optical instruments capable of measuring air data (air speed and direction along with air density and temperature) and warning of icing conditions, all using a common flush-mounted window without protruding into the flow around the aircraft and without ports or probes that can clog with debris or ice up. Military and civil aviation, both fixed- and rotary-wing, would benefit from the additional safety and security of these threat-warning and air-data capabilities.

9.5 Applications

RIDES will be critical in providing the pilot with air data and icing conditions during approaches and climbing, and in specific conditions such as high-altitude tropical clouds. In addition, while not critical to NextGen, such instrumentation will also be essential to lower-flying aircraft such as rotorcraft and other low-flying missions such as rescues and missions led by the Coast Guard. An alternate source of air data to the Pitot system would be of obvious benefit to pilots in potential icing situations and will maintain its accuracy in all flight regimes, even with rotorcraft operating at low speeds or hover, which confound present Pitot systems. Even a limited number of aircraft equipped with RIDES technology could be of utility to aviation safety to many aircraft by communicating warnings of icing conditions to other aircraft nearby and forecasters on the ground.

9.6 Conclusion

MAC's Raman Icing Detection System is a Raman-based spectrograph operating in the ultraviolet, intended to detect icing conditions ahead of an aircraft in flight. The results presented here are preliminary and very encouraging and full characterization of the spectrograph will continue. The combination of systems such as OADS and RIDES would provide the pilot with an alternate dataset, independent of Pitot tubes. Other airborne hazards, such as clear-air turbulence and volcanic ash, can also be measured using optical techniques, and would provide fully-characterized atmospheric conditions around the aircraft.

9.7 Acknowledgments

Michigan Aerospace Corporation acknowledges NASA's support for this SBIR work under the guidance of Larry Goins, Program Manager for this effort, and Dr. Ivan Clark.

9.8 References

9.1. Ryerson, Charles C.: Remote Sensing of In-Flight Conditions: Operational, Meteorological, and Technological Considerations. ERDC/CRREL M–00–1 (NASA/CR—2000-209938), 2000.
9.2. Park, Sun-Ho, et al.: Selecting Characteristic Raman Wavelengths to Distinguish Liquid Water, Water Vapor, and Ice Water. J. Opt. Soc. Korea, vol. 14, no. 3, 2010, pp. 209–214.
9.3. Avila, G., et al.: Ro-vibrational Raman Cross-Sections of Water Vapor in the OH Stretching Region. J. Mol. Spectrosc., vol. 196, 1999, pp. 77–92.
9.4. Sun, Qiang; and Zheng, Haifei: Raman OH Stretching Vibration of Ice Ih. Prog. Nat. Sci., vol. 19, 2009, pp. 1651–1654.
9.5. D'Arrigo, G., et al.: Raman Scattering and Structure of Normal and Supercooled Water. J. Chem. Phys., vol. 75, 1981, p. 4264.

Glenn Research Center
National Aeronautics and Space Administration
Cleveland, Ohio, January 03, 2017